Numerical modelling of hydrodynamic responses of Ocean Farm 1 in waves and current and validation against model test measurements

Jingzhe Jin[1], Biao Su[1*], Rui Dou[2], Chenyu Luan[3], Lin Li[4], Ivar Nygaard[1], Nuno Fonseca[1], Zhen Gao[3]

1. SINTEF OCEAN, Trondheim, Norway
2. Schlumberger Oilfield Equipments (Shanghai) Co., Ltd., Shanghai, China
3. Norwegian University of Science and Technology, Trondheim, Norway
4. University of Stavanger, Stavanger, Norway

Abstract

With the continuous growing of the aquaculture industry and increasingly limited fish farming sites at close to shore areas both in Norway and worldwide, there is a need to develop fish farms suitable for aquaculture production in typical offshore environments. For this purpose, SALMAR has developed and deployed the Ocean Farm 1 facility for offshore fish farming.

The main purpose of this paper is to develop a reliable numerical model and investigate the motion responses of the Ocean Farm 1 structure in waves and current. The established numerical model consists of the Ocean Farm 1's frame structure (with rigidly-connected circular column components), the net and the mooring system. The hydrodynamic external loads and coefficients of the frame structure are obtained by using potential flow theory. The quadratic drag load on the individual circular columns of the frame structure is formulated by a given drag coefficient. The loads on the net are formulated by using the screen model, where the Reynold number dependent lift and drag forces are formulated as a function of the solidity ratio Sn of the net, relative inflow angle and velocity. The hydrodynamic loads on the mooring lines are formulated using the Morison's equation and the structural responses of the mooring lines are obtained using a nonlinear FE model.

With the developed numerical model, time domain simulations are performed. The simulation results are firstly validated against measured data from the decay tests, current tests, and regular wave tests. After the validation, numerical simulations are performed in different irregular wave and current combined weather conditions and the obtained motion response of Ocean Farm 1 are discussed and compared with available measurement data.

Keywords: Ocean farming concept; Hydrodynamic responses; Numerical modelling; Model test measurements

1. Introduction

Aquaculture of salmon in the coastal area started in the 1970s. Ove Grøntvedt and Sivert Grøntvedt set out 20,000 salmon smolt in a floating octagonal fish cage in the coastal area of Laksåvika, Hitra, Norway, in 1970 [1]. This fish cage is recognized as the first floating salmon fish farm in the world. At water surface level, the fish cage has a floating platform to provide buoyance and working space. Flexible net is connected to the floating platform. The shape and volume of the fish cage is kept by using vertical columns. Over the years, this concept has developed to the most dominant concept for the farming of Atlantic Salmon in Norway and worldwide. Nowadays, such a cage system consists of a floating collar with two concentric tubes, flexible net enclosures containing fish, a bottom ring, wires/ropes to connect the floating collar and bottom ring and a weight system at the lower end of the cage to keep sufficient volume within the cage. The system is often

* Corresponding author. SINTEF Ocean, Trondheim, Norway. *E-mail address*: biao.su@sintef.no (B. Su).

moored with a complex mooring system with bridle lines, frame lines, anchor lines and supported buoys. An illustration of such a flexible gravity cage is shown in Fig. 1.

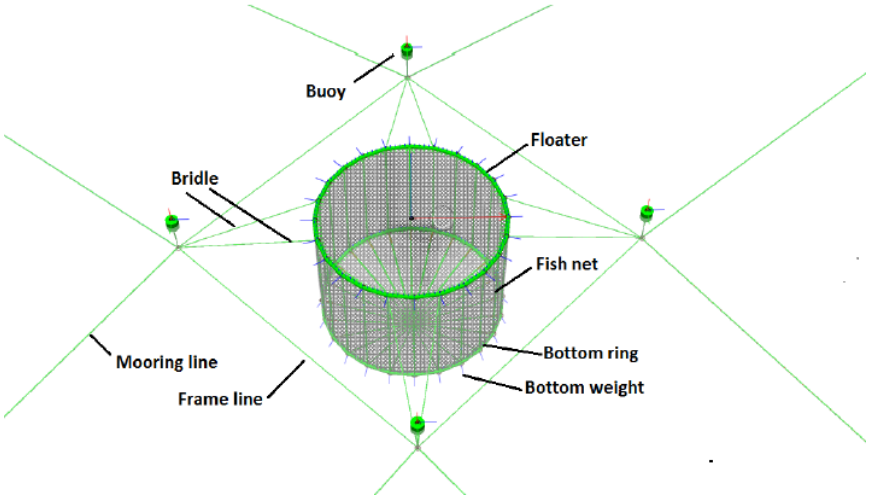

Fig. 1. Illustration of typical flexible gravity cage.

The aquaculture production in Norway today has grown to ten times of the value in 1990 and the same trend is observed worldwide. The continuous growth of marine fish farming has led to a lack of new available sites in sheltered waters, and therefore a gradual move towards more exposed coastal and offshore areas has started. Exposed fish farming requires novel technical solutions suitable for the possible critical conditions that occur on a more severe and frequent basis. On the one hand, the existing types of fish farm structure have to be upscaled and strengthened to take the environmental load at an exposed location [2-3]. On the other hand, several innovative concepts for offshore fish farming are emerging today to provide more robust and cost-efficient solutions when moving further offshore [4]. Many of the concepts have been developed by combining technologies from the fish farming and offshore industry, such as the vessel-shaped "Havfarm" concept, the "Arctic Offshore Farming" concept, the "Egg" closed cage concept and the semi-submersible "Ocean Farm 1" concept. These four concepts are illustrated in Fig. 2.

(a) Havfarm Concept
https://www.nordlaks.no/pressekit-havfarm

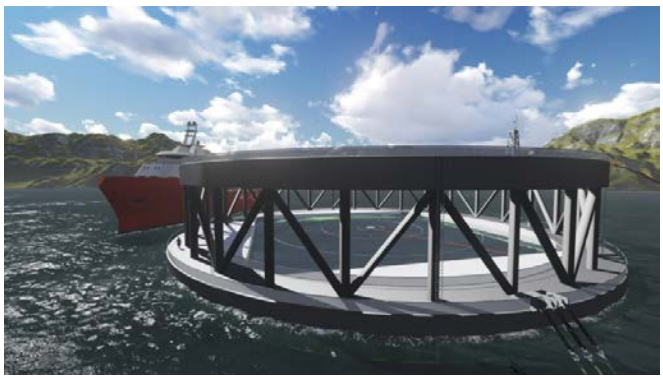

(b) Arctic Offshore Farming Concept
https://norwayroyalsalmon.com

(c) Egg concept
https://haugeaqua.com

(d) Ocean Farm 1 Concept
https://www.salmar.no

Fig. 2. Illustration of four new concepts for offshore fish farming.

Response analysis of a flexible gravity cage system faces several challenges, including the hydrodynamic load and structural modelling of the net, combined hydrodynamic and hydro-elastic response character of the floating collar, convergence issue when net experiences large deformation and inflow reduction effect for the net at leeward side. Analysis of net structures interacting with the surrounding fluid flow is a highly complex, nonlinear hydro-elastic problem where the deformation of the net depends on the hydrodynamic loads, and vice versa. Due to geometry of the net consists of millions of slender twines, a complete fluid-structure interaction analysis is not feasible today. State-of-the-art engineering tools to study aquaculture nets typically apply two main types of semi-empirical hydrodynamic load models: the so-called Morison type and screen type.

The first type is based on the Morison's equation, expressing drag forces on cylinders, and summing up the contribution from each twine independently. The model does not account for hydrodynamic interaction of the twines, but the effects of Reynolds number can be incorporated on twine level. With the Morison model, the Morison's equation is applied to calculate the force for each equivalent net twine. Studies using the Morison model were reported in [5-8], for examples. The screen method may in part account for fluid–structure interaction and integrated flow effects on twine level by using semi-empirical force coefficients for the screens, i.e. net panels [9]. With the screen model, the complete net structure is divided into a number of net panels. The lift and drag force on each net panel are determined using empirical formulas, which are functions of net solidity ratio, inflow angle and Reynolds number. Løland [10] presented empirical formulas for the drag and lift on planar net panels. The formula was determined by curve fitting experiments data of net panel towing tests [11]. The formula given in [10] are functions of solidity ratio in the range of 0.13-0.31 as well as the inflow angle, which was further generalized to include the Reynolds number dependency for solidity ratio smaller than 0.5 in [9]. Studies using the screen model were reported in [12-15], for examples.

For the structural modelling, truss model was originally proposed in [16] and the same truss model was later used in [9 ,14], for examples. Line model was used in [17] to model net panel and the line model was applied in [18] to study cage and vessel interaction. The floating collar of a flexible gravity cage often consists of two semi-submerged concentric tubes, and they have both rigid and elastic motion. Studies on the hydrodynamic response of floating collars in waves and current can be found in [19-21]. The experimental study on flexible net dates back to the 1950s. Experimental data from wind tunnel tests for the forces acting on screens inclined to a steady ambient flow are reported in [22, 23]. Experimental studies on the forces on net panels through towing tests in water were reported in [11, 24-28]. Experimental studies on the response of complete 3D flexible gravity cages are report in [24, 29-31].

The "Havfarm" concept cage is made of a vessel shaped floater, five flexible cages under the floater and mooring and DP system, with a total length of 400 m. The design of the floater is to obtain minimum motion at an offshore location. A single point mooring system design is applied for the "Havfarm" system. Available experimental and numerical study on the "Havfarm" concept were reported in [32,33]. "Arctic Offshore Farming" is a rigid semi-submersible fish farm comprising one upper and one lower circular pontoon with vertical and diagonal bracing between them. Flexible net is attached to the lower pontoon. It has a diameter of 79 m and weighs 2,500 metric tons. The cage can be totally submerged to minimize the exposure to wave loads and it is designed to resist severe wave conditions with Hs 15 m. A preliminary response analysis of such semi-submersible concept was presented in [34]. The "Egg" concept is an ovaloid shaped conceptual design. The 'Egg" concept is 44 m high and 33 m wide and has capacity to hold 1000 tons of salmon. It is a closed cage and the salmon louse will have great difficulty to enter the system. Moreover, the closed concept makes the containment and feeding regimes more accurate. As the intake and outflow of water is separate, the infection pressure among different units in a fish farm is greatly reduced. To the authors' knowledge, there is no published numerical or experimental study on these two concepts: "Arctic Offshore Farming" and the "Egg" concept.

Numerical studies on the Ocean Farm 1 type of structure were also performed in [35, 13]. In [35], nonlinear finite element program USFOS [36] was applied to establish the numerical model of the complete farm-mooring system. Morison's equation was applied to formulate hydrodynamic load on the circular column structure (vertical columns, braces, beams and pontoons). Løland's formula [10] was used to formulate the hydrodynamic load on the net structure. All circular column structures were modelled as beams. For the structural modelling of the net, a simplified model of the net with much coarser mesh was first established and tubular beam elements were used to model individual net twines in the simplified net structure. Ultimate Limit State and Fatigue Limit State analysis were performed for the integrity of the farm-mooring system. In [13], SIMO/SIMA [37, 38] was used to establish the farm – mooring system model. Hydrodynamic coefficients of the circular column structure (vertical columns, braces, beams and pontoons) were calculated using HydroD [39]. Viscous load on the circular columns were modelled using the slender element in SIMO. Løland's formula [10] was used to formulate the hydrodynamic load on the net structure. The load on the net structure was input into SIMO through Dynamic Link Library (DLL). Response of the farm-mooring system was analyzed in current and regular waves. Experimental studies of the response of Ocean Farm 1 type of structure were performed in [40, 41]. In these tests, the complete farm – mooring system were modelled, and the system response was measured in waves and current.

The present paper further develops the work done in [13]. The main improvements lie in: 1) the net force model has been improved to include Reynolds number dependence [9]; 2) The DLL algorithm is upgraded to include irregular wave scenarios and 3) difference frequency force QTF (Quadratic Transfer Function) is calculated and applied in the motion response calculation for the farm structure. In addition, the calculated response of the farm system is systematically validated against measured results as reported in [40].

In summary, the present paper is organized as follows. The structural layout and properties of Ocean Farm 1 – mooring system is described in the first place. Next, the performed model tests are presented including test setup, main measurement, and relevant test matrices. The theoretical background of the problem and numerical modelling of the farm-mooring system are then introduced. After this, the numerical calculation results of the farm motion response are presented, together with comparison against measured data including tests in calm water, in current only condition, in regular waves and irregular waves. At the end, a brief summary of the numerical modelling and simulations results is made, and future work is suggested.

2. Materials and methods

2.1. Structural layout and properties of Ocean Farm 1

Flexible gravity cages with floating collar and flexible net structure often have large deformation under wave and current loads. At an offshore site with high sea states, large cage deformation is considered a critical issue for the gravity cages. To overcome this, SALMAR developed the Ocean Farm 1 concept for offshore fish farming, as illustrated in Fig.3. Rigid frame structure and Econet are chosen for the Ocean Farm 1 structure, in order to resist the excessive environmental loads at the offshore locations and reduce the cage deformation. Econet has a very hard surface to resist fouling and makes it easy to clean in water. It can stay in water for up to 14 years and is widely used in salmon farming.

The full-scale pilot farm was built in 2017, transported to Norway by a special cargo vessel and further towed to its deployment location at Frohavet in the Norwegian Sea by three anchor handling tugs in September 2017. Water depth at the site is 150 m. Operation was commenced in the same month by filling up of one million salmon smolt. The first generation of salmon from the pilot farm was harvested in January 2019. The 100-year condition in which the concept was designed to operate in is: Hs=5 m, Tp=11 s; wind velocity 30 m/s and current velocity 0.75 m/s.

The main particulars of the Ocean Farm 1 are summarized in Table 1. It has a dodecagonal shape when viewed from the above and 12 horizontal columns formulating the upper frame and 12 horizontal columns for the lower frame. There are 12 vertical columns connecting the upper and the lower frames. 6 of the 12 vertical columns have larger diameter than the rest and have pontoons at their lower ends. It also has a central column with a bottom pontoon and the topside is built on top of the central column. 12 inclined braces connect the lower frame to the central pontoon. On the upper frame of the farm, there are two perpendicular main cross braces. On each side surface formulated by the upper frame, the lower frame and the two adjacent vertical columns, there is one diagonal column. Two adjacent diagonal columns share one common end point.

The farm has one movable and two fixed bulkheads to divide the volume into 3 compartments for different operations. The bulkheads connect the central column and the individual side vertical columns. The two fixed bulkheads are connected to column 10 and 11, respectively. During the model tests, the movable bulkhead is connected to column 5.

Econet is attached to the side, bottom and the three bulkheads of Ocean Farm 1. Applied Econet is shown in Fig.4. It is stiffer than traditional net fibres and has relatively low weight. Net particulars are listed in Table 2.

The mooring system of Ocean Farm 1 consists of eight 1100-meter-long catenary lines. A pair of 2 mooring lines are connected to a common fairlead at one side column as shown in Fig. 3c. The fairleads are 14 m above the farm's base line. The angle between the two lines in one pair is 45 degrees. Each catenary line consists of fibre rope at the top and chain at the lower and bottom part. Properties of the catenary lines are summarized in Table 3.

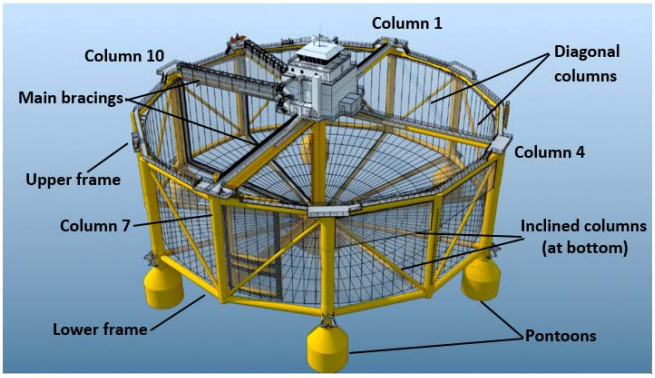

(a) Illustration of Ocean Farm 1 structure

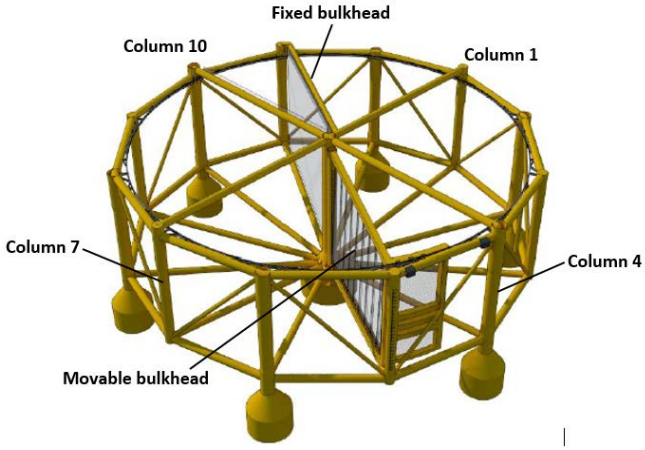

(b) Illustration of the frame of Ocean Farm 1 structure

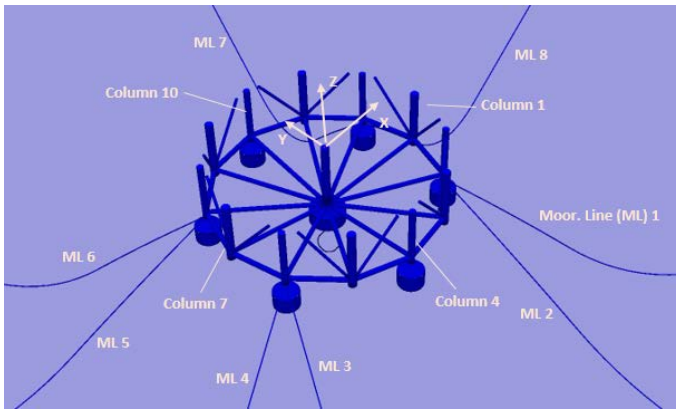

(c) SIMA visualization of the Ocean Farm 1 model

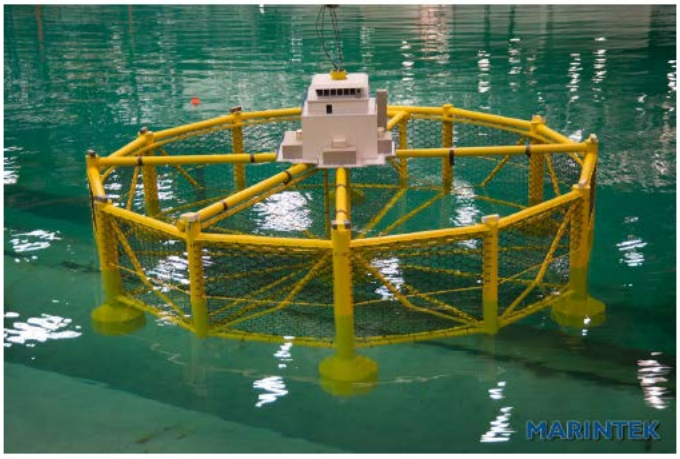

(d) Ocean Farm 1 model in model tests [40]

Fig. 3. Ocean Farm 1 structure and the modelling in SIMA.

Table 1

Ocean Farm 1 Main Particulars [40].

Dimension	Unit	Value (full-scale)
Overall height	m	68
Diameter	m	110
Operation draft	m	43
Vertical center of gravity VCG (from Based line)	m	17.8 / 15.5 [1)]
Roll radius of gyration	m	38/42[2)]
Pitch radius of gyration	m	38/42[2)]
Yaw radius of gyration	m	48/50[2)]
Volume capacity for fish farming	m^3	250,000
Displacement	m^3	13,616
Capacity	-	1 million salmon (approx.)

1) 17.8 m is given in the model test report [40]. 15.5 m is applied in numerical modelling.
2) Roll and pitch radius of gyration is given for axes passing COG. Radius of gyration for roll, pitch and yaw are 38 m, 38 m and 48 m as given in the model test report [40]. In the numerical modelling, the radius of gyration for roll, pitch and yaw are 42 m, 42 m and 50 m, respectively.

The COG position and moment of inertia in the numerical model are slightly tuned to match the measured natural period of heave, pitch and roll.

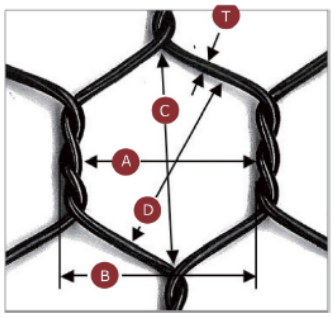

- A = Mesh width
- B = Mesh pitch
- C = Mesh height
- D = Mesh diagonal
- T = Wire thickness

Fig.4. Illustration of the netting structure (Econet: https://www.akvagroup.com/pen-based-aquaculture/pens-nets/nets-/econet)

Table 2

Econet particulars.

Wire diameter T	Mesh width A	Mesh pitch B	Mesh height C	Mesh diagonal D	Weight	Solidity Ratio Sn
3 mm	45 mm	50 mm	71 mm	59 mm	590 g/m^2	0.161

Table 3

Properties of mooring lines [40].

Property	Unit	Chain link	Fiber rope (the top part of each line)
Length	m	1000	100
Diameter	mm	76	130
Elasticity EA	kN	0.508E+06	0.147E+06
Breaking strength	kN	13573	12560
Submerged weight	kg/m	100.5	3

2.2. Model tests of Ocean Farm 1 in waves and current

The model test for the Ocean Farm 1 model was performed in the ocean basin at SINTEF OCEAN in 2014 [40]. The applied model scale is 1:30. All measurements and parameters are presented in full scale hereafter, unless otherwise indicated. Froude scaling with geometric similarity was assumed for the structures except for the net twines. Due to the small net twine diameter, geometric similarity for the net twines cannot be realized. Full scale Econet is applied in the scaled model, with its dimensions given in Table 2. With the full scale Econet applied, the difference of Reynolds number in model and full scale is only related to relative velocity for net structure. This reduces the scale effect of viscous forces due to different Reynolds numbers. Two layers of Econet are inserted in the upper 10m part of all vertical sides of the farm. Solidity ratio and the Reynolds number of the twines are the two important parameters for estimating the drag load on the fish net. Here the solidity ratio Sn is defined as the ratio between the projected area of the net twines of a net screen and the total area of the screen. The solidity ratio Sn for the applied Econet is 0.16. For a relative inflow velocity 0.5 m/s, the Reynolds number for the net twin is 270 in model scale and is 1500 in full scale, for example.

Two coordinate systems are applied: one global and one local systems. The global coordinate system is defined with its origin at the farm's centre on the calm water surface. As illustrated in Fig. 3c, the global coordinate system has the X, Y and Z axis pointing toward the forward, portside and upward directions, respectively. The local coordinate system is a fish farm fixed system. The local coordinate system coincides with the global one in calm water condition, and it follows the fish farm's motion in wave, wind and current. Roll and pitch motions, accelerations and relative wave measurements are referred to the local coordinate system while the remaining measurements are referred to the global coordinate system.

The motion of the fish farm was measured using optical-electronic OQUS position measuring system, which consists of light-emitting diodes on the model and onshore cameras. Force transducers were installed to measure the total horizontal force (Fx and Fy) and yaw moment (Mz) at the fore and aft positions, in pull out tests. For those tests with catenary mooring system, line tension was measured in the upper ends of the 8 mooring lines. Measurement to be applied in this study are summarized in Table 4.

The eight catenary mooring lines were identically made according to the specification. The lines had to be shortened to fit into the Ocean Basin and the anchor positions are revised accordingly. However, the horizontal restoring properties of the shortened mooring system is kept the same as the actual mooring system. The pretension of each mooring line was in the range of 150-200 kN.

With the catenary mooring system, pull out / decay tests, current tests, pink noise and irregular wave tests were performed, which are also numerically simulated in this work. The restoring force test was carried out by pulling the fish farm model to different offset positions while the model's offset and restoring force from the mooring system were measured. Motion decay test was performed in all DOFs except for yaw motion. In the current tests, the current induced force and fish farm offset were measured. Pink noise wave spectra tests were performed to obtain fish farm motion transfer functions. All irregular wave tests were performed with collinear weather condition with duration of 3 hours. Tests applied for the numerical study are summarized in Table 5.

Table 4

List of relevant measurements taken in model tests.

No.	Measurement name	unit
1	Current speed	m/s
2	Surge motion of the farm	m
3	Sway motion of the farm	m
4	Heave motion of the farm	m
5	Roll motion of the farm	deg
6	Pitch motion of the farm	deg
7	Yaw motion of the farm	deg
8	Restoring force along x axis (fore and aft horizontal mooring group)	kN
9	Restoring force along y axis (fore and aft horizontal mooring group)	kN

Table 5

List of relevant test program.

Test type	Definition	Comments
Pull out test	In line	
Pull out test	In between	
Decay tests	Surge	
Decay tests	Sway	
Decay tests	Heave	
Decay tests	Roll	
Decay tests	Pitch	
Current tests	Vel 0.25 m/s, dir. 0 deg	
Current tests	Vel 0.5 m/s, dir. 0 deg	
Current tests	Vel 0.75 m/s, dir. 0 deg	
Irregular wave, no current	Hs 5 m, Tp 11 s, dir. 0 deg	In line
Irregular wave, no current	Hs 4 m, Tp 10 s, dir. 0 deg	In line
Irregular wave, no current	Hs 3 m, Tp 9 s, dir. 0 deg	In line
Irregular wave, no current	Hs 1.5 m, Tp 7 s, dir. 0 deg	In line
Irregular wave, with current	Hs 5 m, Tp 11 s, current vel. 0.75 m/s, dir. 0 deg	In line
Irregular wave, with current	Hs 4 m, Tp 10 s, current vel. 0.75 m/s, dir. 0 deg	In line
Irregular wave, with current	Hs 3 m, Tp 9 s, current vel. 0. 5 m/s, dir. 0 deg	In line
Irregular wave, with current	Hs 1.5 m, Tp 7 s, current vel. 0.25 m/s, dir. 0 deg	In line

2.3. Numerical modelling of Ocean Farm 1

Potential flow hydrodynamic loads on the Ocean Farm 1 are calculated using the boundary element method. The hydrodynamic response calculation of an aquaculture unit is important both in the design phase and operation phase. For flexible gravity cage consisting of floating collar, bottom ring, net and bottom weight, the challenges lie in the dominating hydro-elastic responses, the large number of net twines and the partial submergence of floating collars. The Ocean Farm 1 is a semi-rigid structure. The frame structure of Ocean Farm 1 is rigid, and it consists of many circular columns and several pontoons. The Econet attached on the frame is semi-rigid, which only deflects to some extent. Unlike the elastic response of the flexible gravity cage structure, the Ocean Farm 1 structure behaves more like a rigid body subjects to environmental loads. Therefore, in the numerical simulations, the frame structure and the attached net are considered as one rigid body, while the mooring system is modeled as flexible structures.

In this section, the theories and the assumptions applied in analyzing the response of Ocean Farm 1 with mooring line system are presented. This mainly includes the theoretical models for Ocean Farm 1's frame structure, the nets and the mooring system.

2.3.1. The frame structure

Potential flow hydrodynamic loads on the Ocean Farm 1 are calculated using the boundary element method. With the low-order method in WAMIT [42], the body wetted surface at mean position is discretized into a set of quadrilateral panels. Here the body wet surface corresponds to the part of the frame structure under mean water surface level and excludes the door frame of the movable bulkhead, as shown in Fig. 3c. The radiation and diffraction velocity potentials are assumed to be constant across each panel. Based on this discretization, the continuous integration equations are transformed to a set of linear simultaneous equations, with the radiation and diffraction potentials to be the unknowns. Once the velocity potentials are solved, fluid particle velocity and fluid pressure become known as well. The forces and moments on the body due to radiation and diffraction are then obtained by integrating the pressure on the wet surface.

The frame structure consists of many circular columns. The viscous load on these circular columns influences the motion response of the frame structure. To consider the viscous load effect, dummy slender element is added on each column in the numerical modelling in SIMO/SIMA. The dummy slender element has the same dimension as the column and a drag coefficient is specified for each added slender element (the column). Added mass force on these columns is not included since it has already been considered in the hydrodynamic response calculation in WAMIT. The viscous effect on all the circular columns as shown in Fig. 3c is taken into consideration in SIMO time domain simulations.

2.3.2. The net

The experimentally based screen type of force model [9] is used to calculate the hydrodynamic and viscous forces acting on the net. It is assumed that the total load on the complete net structure can be represented by the superposition of the individual loads on a set of net panels/screens.

The mean drag and lift force on a net panel depends on solidity ratio, Reynolds number, and the relative inflow direction and velocity. The inflow direction/angle is defined by the angle between net normal vector and the relative inflow vector. The drag force on a panel is along the direction of relative inflow vector and the lift force direction is perpendicular to the relative inflow vector and at the cut between plane 1 (defined by normal net vector and the relatively inflow vector) and plane 2 (normal to the relative inflow vector) [43]. The drag and lift coefficients are determined based on experiments with net panel in steady flow [10, 11].

In addition to the lift and drag forces, inertia forces applied on net panel can be included in a similar manner as in the Morison’s formula [44]. Experimental work has shown that the inertial forces on net structure can be

important, though viscous forces dominates [25]. In the current work, the inertia forces on the net is not considered.

The screen force model [9] was originally developed for steady flow, and it was shown to give clear improvements in calculating the drag and lift forces on the net cages in current as compared with a Morison type of force model [45]. Due to the high Keulegan-Carpenter number with respect to the twine diameter, the flow in waves can be assumed as quasi-steady, thus the screen force model is considered also applicable in waves [31].

The model divides the net structure into a number of flat net panels, or screens. The total load onto each net panel is calculated using the relative velocity and direction at its centre point. And the total load onto the net structure is a superposition of the load onto all the net panels. Each net panel is assumed to experience a viscous normal force, $\mathbf{F}_N \in \mathrm{P}^3$ (3D vector), due to a pressure drop proportional to the square of the instantaneous, relative flow velocity, $\mathbf{U}_{rel} \in \mathrm{P}^3$, and a tangential force, $\mathbf{F}_T \in \mathrm{P}^3$, due to the flow deflection by the net twines when going through the net. The resultant force can be, alternatively, decomposed into the drag force, $\mathbf{F}_D \in \mathrm{P}^3$, and the lift force, $\mathbf{F}_L \in \mathrm{P}^3$, as shown in Fig. 5. The non-dimensional drag and lift force coefficients are defined as:

$$C_D = \frac{|\mathbf{F}_D|}{0.5\rho A|\mathbf{U}_{rel}|^2} \tag{1}$$

$$C_L = \frac{|\mathbf{F}_L|}{0.5\rho A|\mathbf{U}_{rel}|^2} \tag{2}$$

where ρ is the water density, A is the panel area. The instantaneous, relative flow velocity, $\mathbf{U}_{rel}$ is written as:

$$\mathbf{U}_{rel} = r\mathbf{U}_\infty + \mathbf{U}_w - \dot{\mathbf{x}}_i \tag{3}$$

where $\mathbf{U}_\infty \in \mathrm{P}^3$ is the incoming current velocity, r is the velocity reduction (wake) factor, $\mathbf{U}_w \in \mathrm{P}^3$ is the total wave particle velocity at the position of the node and $\dot{\mathbf{x}}_i \in \mathrm{P}^3$ is the velocity of the node. The practical importance of the velocity reduction is that the rear part of the cage will experience a reduced inflow, as described in [10]:

$$r = 1 - 0.46c_d^{net.0} \tag{4}$$

where $c_d^{net.0}$ is the calculated drag coefficient for a vertical net panel. The wake effect for the oscillatory flow is difficult to be incorporated, thus it is often assumed that only the steady part of the flow, i.e. the current, is reduced as shown by Shen [46].

The experimental data from Goldstein [47] was used in [9] to represent the drag coefficient of a circular cylinder, $C_D^{cir.cyl}$, as a seventh order polynomial of $\log_{10}\mathrm{Rn}$ for the Reynolds number range $10^{3/2} \le \mathrm{Rn} \le 10^4$:

$$\begin{aligned} C_D^{cir.cyl} = \quad & -78.46675 + 254.73873(\log_{10}\mathrm{Rn}) - 327.8864(\log_{10}\mathrm{Rn})^2 \\ & + 223.64577(\log_{10}\mathrm{Rn})^3 - 87.92234(\log_{10}\mathrm{Rn})^4 + 20.00769(\log_{10}\mathrm{Rn})^5 \\ & - 2.44894(\log_{10}\mathrm{Rn})^6 + 0.12479(\log_{10}\mathrm{Rn})^7 \end{aligned} \tag{5}$$

For a flat net panel, the Reynolds number is defined as:

$$\mathrm{Rn} = \frac{|\mathbf{U}_{rel}|d_w}{\nu(1-\mathrm{Sn})} \tag{6}$$

where d_w is the net twine diameter and ν is the kinematic viscosity of water. The drag and lift coefficients may formally be represented by the Fourier series of θ, which is the angle between $\mathbf{U}_{rel}$ and the normal of the net panel. One approximation is to keep the first two terms in each series, i.e.

$$C_D(\theta) = c_d^{net.0}(0.9\cos\theta + 0.1\cos 3\theta) \quad (7)$$

$$C_L(\theta) = c_l^{net.45}(1.0\sin 2\theta + 0.1\sin 4\theta) \quad (8)$$

where

$$c_d^{net.0} = C_D(0) = C_D^{cir.cyl}\frac{\mathrm{Sn}(2-\mathrm{Sn})}{2(1-\mathrm{Sn})^2} \quad (9)$$

$$c_l^{net.45} = C_L(\pi/4) = (0.5c_d - \frac{2\pi c_d}{32+2c_d})/\sqrt{2} \quad (10)$$

Eqs. (7-10) relate the drag and lift coefficients of a net panel to the Reynolds number dependent drag coefficient of a circular cylinder, which are applicable for $10^{3/2} \leq \mathrm{Rn} \leq 10^4$, $\mathrm{Sn} \leq 0.5$ and $0 \leq \theta \leq \pi/2$. A thorough description of these formulations and the corresponding parametric studies can be found in [9].

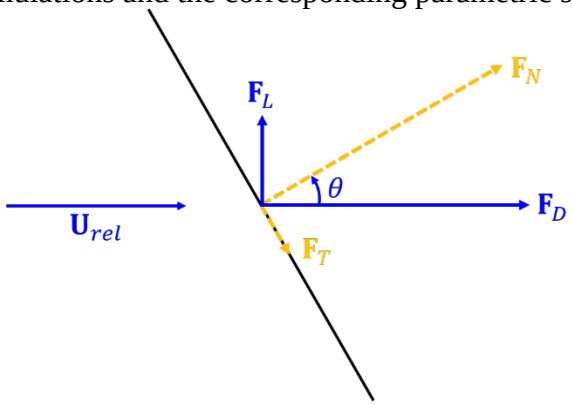

Fig. 5. Drag (F_D) and lift (F_L) forces on a net panel. θ is the angle between the normal of the net panel and the direction of the instantaneous, relative flow velocity, U_{rel} . F_N and F_T denote the corresponding normal and tangential components of the hydrodynamic, viscous forces.

2.3.3. The mooring system

8 catenary mooring lines are applied to keep the farm in position, as shown in Fig. 3c. The lines are subject to gravity, buoyancy, hydrodynamic and viscous load in waves and current. The hydrodynamic and viscous loads are formulated using Morison's equation. The lines are modelled using Finite Element Method (FEM). For the part of mooring lines lying on the seabed, seabed contact is modelled to include the vertical support force and friction force on the seabed plane. The mooring system is designed so that it only constrains the slowly varying motion of the farm but not the wave frequency motion. Mooring line dynamics and cage motion are coupled through the connection at the fairleads.

2.3.4. Integrated numerical framework

Based on the theory given in the previous sections, the numerical model of Ocean Farm 1 with mooring system is established by using WAMIT, SIMO and RIFLEX [48] in SIMA environment. The Ocean Farm 1 structure is modelled in SIMO while the mooring line system is modelled in RIFLEX. Coupled SIMO-RIFLEX simulation is performed in the time domain. "Coupled simulation" means that the motion of Ocean Farm 1 structure and the mooring line dynamics are solved simultaneously. The drag force on the frame columns is calculated using the relative velocity between the instantaneous structure motion and fluid motion. The drag and lift forces on the net are calculated using the relative velocity between the instantaneous structure motion

and fluid motion at initial net panel position. The numerical modelling procedures are highlighted in Fig. 6. Details of the numerical modelling procedures are explained and discussed in this section.

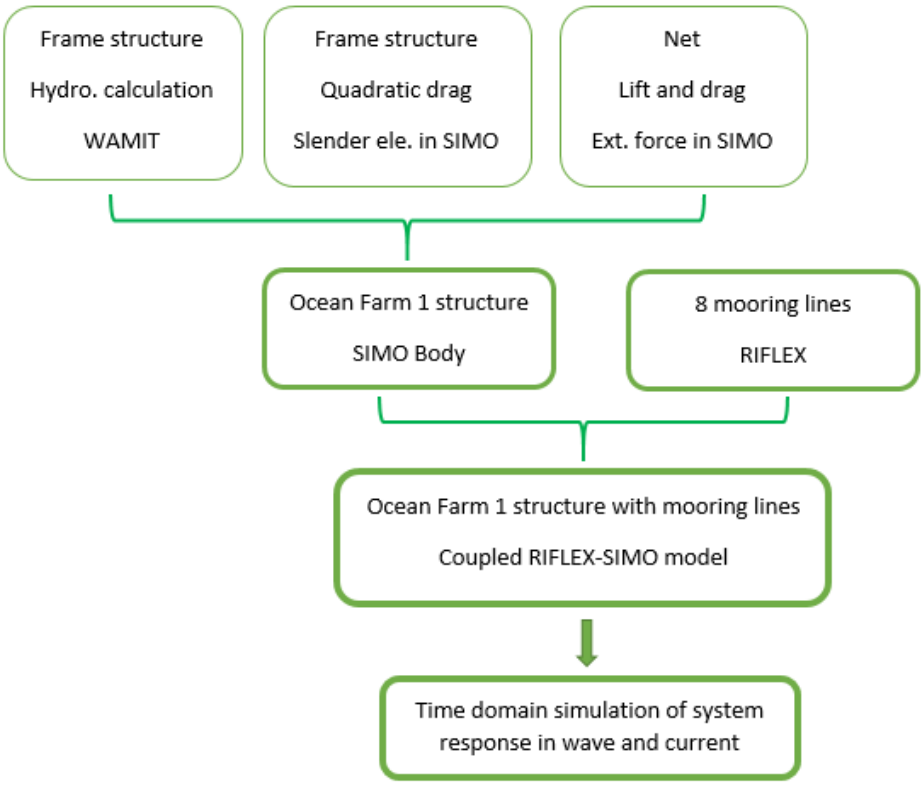

Fig. 6. Flowchart of the numerical modelling of Ocean Farm 1 – mooring line system.

1) WAMIT

The coordinate system applied in WAMIT calculation is located at the calm water surface and with z axis pointing upward. The origin of the coordinate system is at the center of the farm at calm water surface level. The WAMIT calculated motion is referred to the origin of the coordinate system. The panel model together with the coordinate system applied in WAMIT calculation is illustrated in Fig. 7.

There are in total 14632 panels used to discretize the body wet surface. The frame structure's potential flow hydrodynamic coefficients and wave exciting forces are calculated for wave period between 3 s and 40 s and at wave direction between 0 deg and 180 deg with 30 deg interval. Water depth is 150 m. In addition to frequency dependent added mass and damping coefficients and wave excitation force, WAMTI calculation also outputs the transfer functions of wave particle velocities at specified locations. At these locations, the wave particle velocities are needed to formulate the lift and drag force on the net panels.

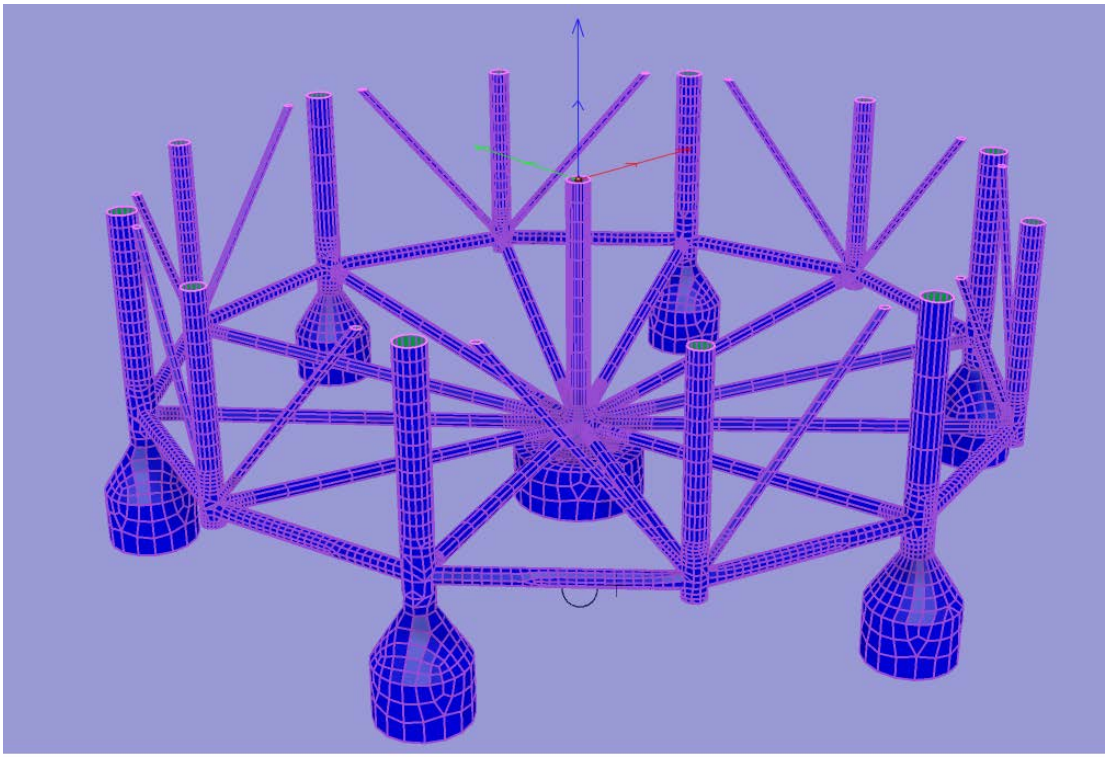

Fig. 7. Panel model of the submerged part of the frame structure of Ocean Farm 1.

2) SIMO

SIMO is a program to perform time domain simulations for stationary floating structures and different marine operations. SIMO provides the option to add external force. The purpose of this function is to consider forces which cannot be directly modelled by SIMO itself. The force on net structure is such an example. Adding external force is realized by using DLL (Dynamic Library Link) in SIMO. SIMO outputs part of the calculation results including current time, step/sub-step number, current velocity, global position and velocity and local total velocities of all bodies at each time step to the DLL. With the SIMO input, the external force (three force components and three moment components) is formulated in the DLL and is returned to SIMO time domain simulation at a specified body point. The time domain calculation then proceeds to the next time step.

The Ocean Farm 1 has 12 pieces of vertical net structures, 12 pieces of bottom net structures and 3 bulkheads with net structures. In this study, each side net structure is discretized into 25 net panels, each bottom net structure is discretized into 16 net panels and each bulkhead is discretized into 25 net panels. SIMO exports the farm's position and velocity at a reference position to the DLL. And inside the DLL, the global motion velocity at the center of each net panel is derived and the unit normal of each net panel is formulated based on the rotation of the farm frame structure as well.

The time histories of the wave particle velocity at the initial center position of each net panel are pre-generated by using incoming wave time history and the WAMIT calculated transfer function of the wave particle velocity at the center point of each net panel. At each time step, the calculated wave particle velocities at the initial net panel center positions are called by the DLL to calculate the total relative velocity for each net panel, together with the global motion velocity of each net panel center and the current velocity. Reduced current velocity is applied for the net at the leeward side, according to Eq. (4). With the total relative velocity, the unit normal of net panel, Reynolds number and solidity ratio, the lift and drag forces on each net panel are formulated. The forces are then transformed into forces in the global coordinate system. And the total force on

net structures is calculated by summing up the lift and drag forces over all the net panels. The DLL then returns the total force applied on net structures back to the frame body defined in SIMO. The total force on the net is updated at each time step when solving the equations of the motion for the whole fish farm.

The added mass force applied on the net structure is not included in the current numerical model, due to its relatively small magnitude. The total mass and volume of the net structure are listed in Table 6.

Table 6

Total mass and volume of the net and the frame structures.

	Net structure	Frame structure	Ratio of Net. Vs Frame
Volume (m3)	1.15E+01	1.25E+04	9.2E-04
Mass (kg)	1.4E+04	1.28E+07	1.1E-03

Full scale Econet is applied in the model tests. With Froude scaling, the Reynolds number for the net in the model tests does not match the Reynolds number for the actual fish farm net. A smaller Reynolds number is experienced by the net during model tests compared to the full-scale case. To illustrate the difference, the drag force coefficients in model and full-scale scenarios are summarized in Table 7 according to Eqs. (5-10), for 0 deg angle between the relative velocity and net normal vector. It is found that the drag coefficient in model scale is about 10-30% larger than the drag coefficient in full scale. Corresponding difference is expected for the lift force coefficient based on Eqs. (5-10). Both full scale and model scale drag coefficients shown in Table 7 are applied in the following numerical simulations. Due to the scale effect, difference between measured farm performance in model tests and full scale farm performance is expected.

Table 7

Drag force coefficient for the net in model scale and full scale (0-degree relative inflow angle).

Full Scale Scenario			Model Scale Scenario			Ratio of MS c_d^{net} and FS c_d^{net}
Rel. vel. (m/s)	Rn	c_d^{net}	Rel. vel. (m/s)	Rn	c_d^{net}	
0.2	7.14E+02	0.22	0.04	1.29E+02	0.28	1.25
0.4	1.43E+03	0.20	0.07	2.57E+02	0.27	1.33
0.6	2.14E+03	0.20	0.11	3.86E+02	0.25	1.27
0.8	2.86E+03	0.20	0.15	5.14E+02	0.24	1.18
1.0	3.57E+03	0.21	0.18	6.43E+02	0.23	1.10

The diameter of the different circular columns ranges from 1 m to 3.5 m. The Reynolds number for the circular columns in model and full scale is listed in Table 8 for a representative column diameter 2 m. In full scale case, the Reynolds number is in the order of [1E+05 1E+06] and in the model tests the Reynolds number is in the order of [2.4E+03 1.21E+04]. This indicates that the drag force coefficients on the columns in model tests can be larger than that in full-scale scenario, which is similar as the drag and lift load on the net structure. Reynolds number and roughness dependent cylinder drag coefficient are presented in Fig. 8 [49]. For painted steel, its surface roughness is 5.0E-06 m and the roughness increases with the service life of the farm structure

at sea. The Reynolds number dependent smooth cylinder drag coefficient is listed in Table 8 as a reference for estimation of the cylinder drag coefficient in the model test and full-scale scenarios.

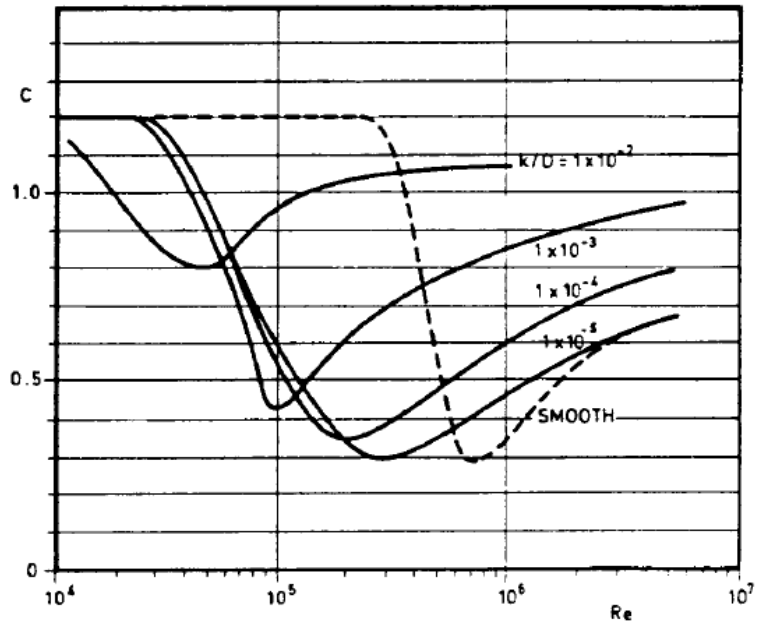

Fig. 8. Drag coefficient for fixed circular cylinder for steady flow in critical flow regime, for various roughness [49].

Table 8

Drag force coefficient for the frame column in model scale and full scale (0-deg attack angle).

Full Scale Scenario (Column Diameter 2 m)			Model Scale Scenario (Column Diameter 2 m)		
Rel. vel. (m/s)	Rn	Smooth cylinder drag coefficient	Rel. vel. (m/s)	Rn	Smooth cylinder drag coefficient
0.2	4.00E+05	0.9	0.04	2.42E+03	1.2
0.4	8.00E+05	0.3	0.07	4.85E+03	1.2
0.6	1.20E+06	0.4	0.11	7.27E+03	1.2
0.8	1.60E+06	0.5	0.15	9.70E+03	1.2
1.0	2.00E+06	0.5	0.18	1.21E+04	1.2

The pontoons and the center bottom column have sharp edges. When the farm has heave, pitch and roll motion, vortex will shed from these edges. The induced viscous loads on the farm structure in the vertical direction are accounted for by using slender elements in SIMO. These slender elements are defined at the actual position of the pontoons/center bottom column and only the drag load in the vertical direction is included. The drag force coefficient $c_d^{vertical} = 1.9$ is applied [49].

3) RIFLEX

RIFLEX solves the hydrodynamic response of slender marine structures, where gravity, buoyancy, and hydrodynamic load due to waves and current based on Morison's equation are considered. The response of the slender structure is solved using FEM method in the time domain, where geometry non-linearity can be considered. The 8 mooring lines are numerically modelled using RIFLEX. Particulars of the 8 mooring lines are given in Table 3.

The 8 mooring lines are grouped into 4 pairs and each pair is connected to one side column as shown in Fig. 3c. The fairlead positions are 14 m above the Ocean Farm 1's base line. The angle between two adjacent mooring lines is 45 deg. The measured and calculated anchor positions for the two-example mooring line no. 7 and 8 are listed in Table 9. Other anchor position can be derived based on the symmetric layout of the mooring system.

Table 9

Measured and calculated anchor positions.

Line no.	X pos. meas.	X pos. cal.	Y pos. meas.	Y pos. cal.
7	432	463	1024	1037
8	1004	1057	452	446

20 bar elements are used to model the 100 m long rope part of the mooring line at the top; 100 bar elements are used to model the 1000 m long chain part of the mooring line at the lower part. The applied quadratic drag coefficient is 1.2 for the rope part of the mooring line and is 2.4 for the chain part of the mooring line. The applied added mass coefficient is 1.0 for rope and 2 for chain part of the mooring lines. Seafloor normal contact is modelled with normal stiffness 5E+04 N/m^2 and the axial and lateral stiffness in the seabed place are modelled with stiffness 1.5E+04 N/m^2. Horizontal axial and lateral friction parameter at seabed is set to 0.6.

The measured and calculated static pretension of each mooring line are summarized in Table 10. The mooring line tensions were measured by strain gauge rings inserted in the upper end of the mooring lines.

Table 10

Measured and calculated static mooring line pretension.

Line number	1	2	3	4	5	6	7	8
Pretension (kN), meas.	175	156	168	189	194	171	169	189
Pretension (kN), num.	146	160	152	150	150	160	150	150

3. Results and discussions

3.1. Comparison of the numerical and experimental results for calm water, current only and pink noise wave conditions

Results of numerical calculation and measurement in calm water, current only and pink noise wave conditions and their comparisons are presented in this section. The focus is on the rigid-body motion of Ocean Farm 1 and the total restoring force from the mooring system. The results of pull out and decay tests are presented in the first place, followed by the results in current and in pink noise waves.

3.1.1. Pull out tests

The static pull out tests were carried out to document the force-displacement behavior of the mooring system. The tests were performed by pulling the Ocean Farm 1 model to different offset positions in two directions: along the X-axis (defined as "InLine" test) and along the direction 45-degree to the X-axis (defined as "InBetween" test). During the tests, the total pulling force, the individual mooring line tension and the position of the fish cage were continuously measured. The largest measured offset of the fish farm is about 25 m away from its initial position. The calculated and measured total pulling force are presented in Fig. 9. The calculated force-displacement behavior agrees well with the measurement, which ensures a good agreement of the total mooring restoring effect on the motions of Ocean Farm 1. The two pulling directions give the same force-displacement behavior, as the mooring line anchor positions are symmetrically arranged.

Fig. 9. Restoring force vs. offset curve, pull out tests.

3.1.2. Decay tests

The decay tests were performed to document the natural periods of the rigid-body motions and damping levels. The calculated and measured natural periods are summarized in Table 11. The measured and calculated surge, heave and pitch decay responses are plotted in Figs. 10-12.

"Cal-Nominal" is with the nominal numerical model where drag load on the frame structure and the drag and lift load on the net are considered (drag and lift force calculated with full scale Reynolds number dependent force coefficients), and "cd" is the drag coefficient applied on the frame columns. Three different values of drag coefficient on the frame columns are applied: 0.4, 0.8 and 1.2. To understand the influence of the different force components, two more numerical models are prepared: one is with net force calculated based on model scale Reynolds number dependent force coefficients to obtain a closer match to the net load measured during model tests and it is denoted as "Cal_MsNetForce cd1.2; the other one is with the net load removed from the nominal numerical model and it is denoted as "Cal_NoNetForce cd1.2". For these two numerical models, the

applied drag coefficient for the frame columns is 1.2. In addition, one more numerical model is prepared to match the measured surge decay performance. And it is found that one has to add about 20% critical surge damping into the nominal model with column drag coefficient 1.2 to obtain a close match between measured and calculated surge decay performance. Some of these cases (three nominal cases; two cases with different net load formulation; one case with nominal model, column drag 1.2 and added surge damping) are also applied in the following studies on current tests and pink noise wave tests. Mooring line damping due to the drag forces on the lines is included in the analysis. To summarize, the numerical models applied in section 3.1.2 and section 3.1.4 are summarized below. The purpose of including these different models is to find a most suitable way to model the measured farm motion.

1) "Cal_Nominal cd0.4", with net load at full scale Reynolds number and column drag 0.4
2) "Cal_Nominal cd0.8", with net load at full scale Reynolds number and column drag 0.8
3) "Cal_Nominal cd1.2", with net load at full scale Reynolds number and column drag 1.2
4) "Cal_N. cd1.2 Added surge damp.", with net load at full scale Reynolds number, column drag 1.2 and additional surge damping added.
5) "Cal_MsNetForce cd1.2", with net load at model scale Reynolds number and column drag 1.2
6) "Cal_NoNetForce cd1.2", without net load and column drag 1.2

The numerical model captures the measured natural periods of the Ocean Farm 1 structure well, as summarized in Table 11. The natural periods are calculated using the nominal numerical model and with frame drag coefficient set to 0.8. The corresponding linear and quadratic damping from measured and calculated decay test are also summarized in Table 11. Quadratic surge damping is underestimated by the current numerical model so that the calculated surge motion decays more slowly than the measurement as shown in Fig. 10. The other damping terms except the surge quadratic damping are reasonably estimated.

The decay performance comparisons show that both the frame drag force and the net force contribute to the surge decay performance. The surge decay performance without net force included is close to that with nominal numerical model and frame column drag coefficient 0.4. The influence of whether using the full scale or model scale Reynolds number to formulate the net force on the surge decay performance is not significant. Change of drag coefficient on the frame columns and different formulations of net load does not influence the heave and pitch decay performance very much because these coefficients mainly act in the horizontal direction. The numerical model seems to underestimate the damping in surge so that additional linear damping must be added to obtain a similar surge decay performance as in the measurement. On one hand, the drag load onto the frame columns and the lift and drag load onto the net structure are formulated by assuming that the interaction between these structure components is not important. However, the interaction influences the farm motion. When these structure components are grouped together, the total force on the overall farm structure can be different from the sum of the individual force onto each structure component. This interaction is not considered in the numerical modelling and this may influence the farm motion performance including surge decay performance, for example. On the other hand, there is scale effect between the model scale and full-scale farm structure and their decay performance can be different. The full-scale farm experiences smaller drag due to the high Reynolds number. Different column drag coefficients are applied in the numerical modelling to illustrate the possible behavior of the full-scale farm. As illustrated in the decay performance comparison, the Reynolds number dependent scale effect of the net load is limited.

Table 11

Measured vs. calculated natural periods, linear and quadratic damping.

DOF	Natural period meas./cal. *	Linear damping coefficient per unit mass meas./cal. *	Quadratic damping coefficient per unit mass meas./cal. *
Surge	175/170 (s)	0.005/0.004 (1/s)	0.37/0.18 (1/m)
Sway	175/170 (s)	0.007/0.004(1/s)	0.37/0.18 (1/m)
Heave	25.5/27 (s)	0.04**/0.02 (1/s)	0.16**/0.19 (1/m)
Roll	29/31.5 (s)	0.03**/0.01 (1/s)	0.18**/0.14 (-)
Pitch	30.8/31.5 (s)	0.03**/0.01 (1/s)	0.18**/0.14 (-)

*The calculated period is with the nominal numerical model frame column drag coefficient cd=0.8

**Formulated based on measured data directly and they are not the same as reported in the model test report [40].

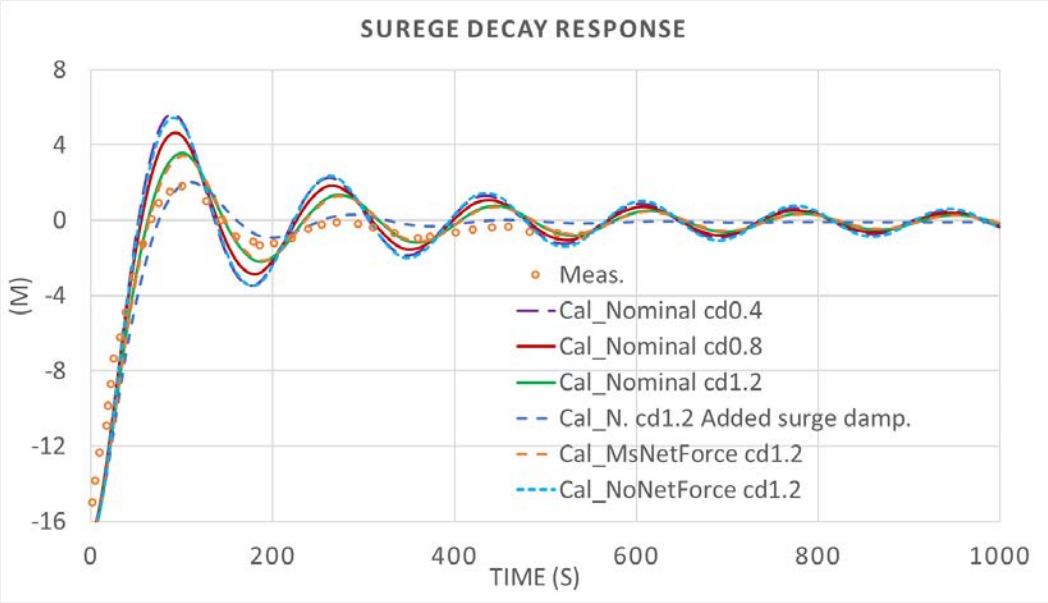

Fig. 10. Surge Decay Responses.

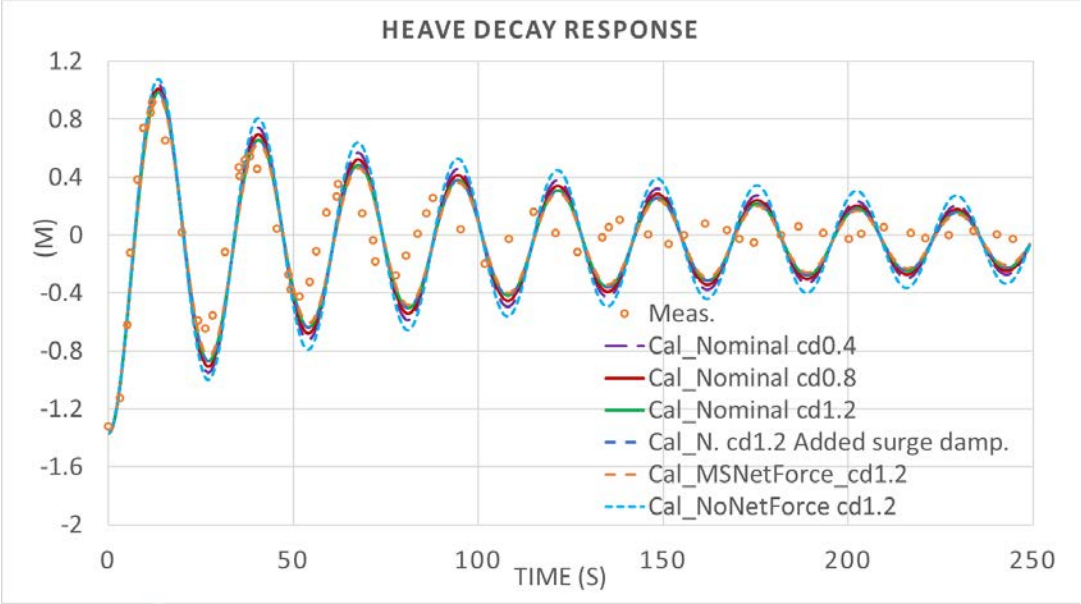

Fig. 11. Heave Decay Responses.

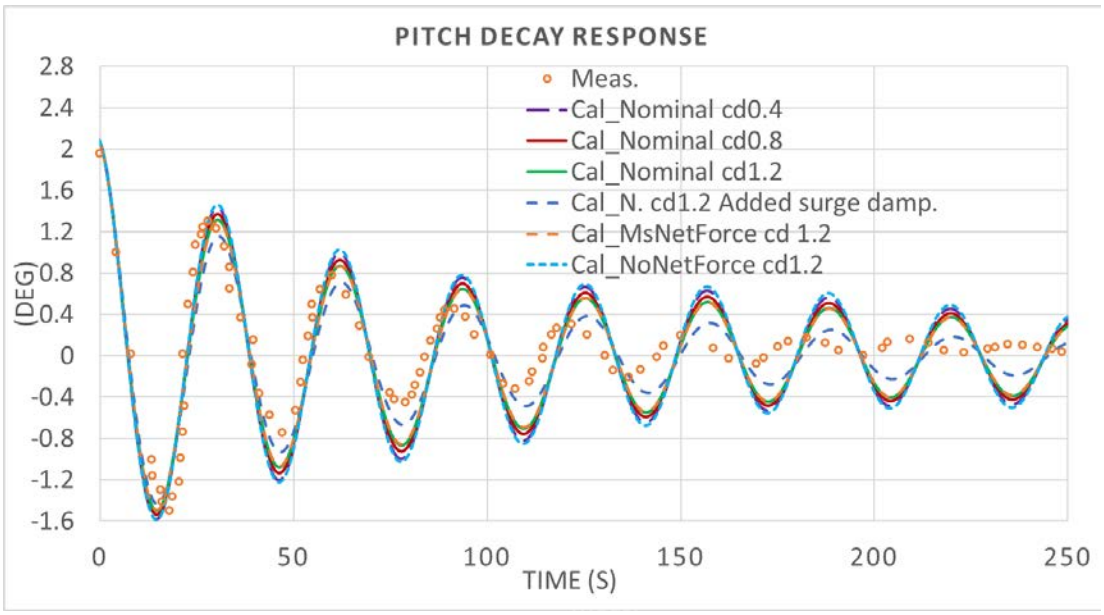

Fig. 12. Pitch Decay Responses.

3.1.3. Current tests

The current tests were performed at three current velocities: 0.25, 0.5 and 0.75 m/s and the current direction is along the negative X-axis. During the tests, both the mooring lines tension and the offset of Ocean Farm 1 were measured. Comparison of the calculated and the measured offset is presented in Table 12. The same 5 cases as studied in the decay test are applied: nominal models with three different drag coefficients for the frame columns and two models with different net load formulations.

With the nominal model and drag coefficient of frame column set to a value between 0.4 and 1.2, the calculated offset generally matches the measurement. In the full-scale situation, the Reynolds number for the circular frame columns is in the range of [4.0E+05 1.6E+06] for the tested current speeds, as shown in Table 8. In this range, the drag coefficient for a circular cylinder normally drops to the minimum value then increase again. In the model tests, the Reynolds number for the frame columns is in the range of [2.4E+03 9.7E+03]

for the tested current speeds, as shown in Table 8. In this range, the drag coefficient is less sensitive to Reynolds number and normally has a constant value close to 1.2. The three nominal models represent the full-scale scenarios and one can apply different frame column drag coefficient at different current velocities to obtain a good estimation of the farm offset, according to Table 8.

The viscous load on the net structure is also dependent on Reynolds number. As the full-scale net is applied in the model tests, the scaling effect (due to different Reynolds number in model scale and full scale) is less significant than the case with a properly down-scaled net model applied, though the scaling effect still exists. This case, "MsNetForce" with cd = 1.2, gives the closest match to the measurement of the model tests, where the frame drag load and net load are both formulated using model scale Reynolds number. For this case, the calculated and measured offset at 0.5 m/s current velocity agrees well; the offset difference at current velocity 0.25 m/s and 0.75 m/s indicates the offset is rather sensitive to the applied drag force coefficients and a further tuning of the coefficients is needed to improve the match against measurement. With the net load removed from the numerical model, the case "NoNetForce" with cd = 1.2, presents the farm's offset due to the frame column drag only.

Table 12

Measured vs. calculated offset of Ocean Farm 1, in current tests.

Current speed (m/s)	0.25	0.5	0.75
Measured offset (m)	8.5	16	22.4
Calculated offset (m), nominal model, cd = 0.4	3.5	12	21.4
Calculated offset (m), nominal model, cd = 0.8	4.3	14.5	23.9
Calculated offset (m), nominal model, cd = 1.2	5.1	16.4	26
Calculated offset (m), ''MsNetForce'', cd = 1.2	5.8	17.5	26.7
Calculated offset (m), ''NoNetForce'', cd = 1.2	2.6	9.8	18

3.1.4. Pink noise wave tests

The Ocean Farm 1 model was tested in pink noise wave spectrum, with no current or wind. The purpose of the test is to understand the Ocean Farm 1's performance in waves with different periods and to obtain the linear motion transfer functions. The wave propagates along the negative X-axis. The pink noise wave spectrum covers period range 5-25 s. For this study, the motion RAOs extracted from pink noise wave with Hs=2.5 m are used for comparison with numerically calculated motion RAOs. The numerically calculated motion RAOs are generated in the same way as those from the model tests through spectrum analysis.

The calculated motion RAO and the measured motion RAO are compared in Figs. 13-15 for surge, heave and pitch motions, respectively. The presented motion RAO is for the reference point at calm water surface and center of the fish farm. The same 5 cases as studied in the decay and current test are applied: nominal models with three different drag coefficients for the frame columns and two models with different net load formulations.

It is observed that the predicted surge, heave and pitch RAOs are generally close to measurement. The surge motion RAO is underestimated in the frequency range [0.05-0.1 Hz] and it is reasonably predicted

outside this frequency range. The measured motion RAOs do not cover the natural frequencies of surge and pitch motion. The calculated motion RAOs indicate: net load plays an important role in the heave motion response at its resonance and limited influence outside the resonance frequency; frame drag coefficient influences the pitch motion at its natural frequency and has limited influences outside the natural frequency.

The RAO comparison indicates that the first order wave frequency motion response of the Ocean Farm 1 structure is dominated by the response of the frame structure based on potential flow analysis. Including the net force and the drag load on the frame structure will mostly change the motion response at their natural frequencies but not the wave frequency motion responses. The proper representation of the net force and frame columns are important when performing simulations in irregular wave, as there will be second order wave force excitation at the resonance frequencies and accurate motion estimation depends on a proper drag force estimation for the frame columns and the net.

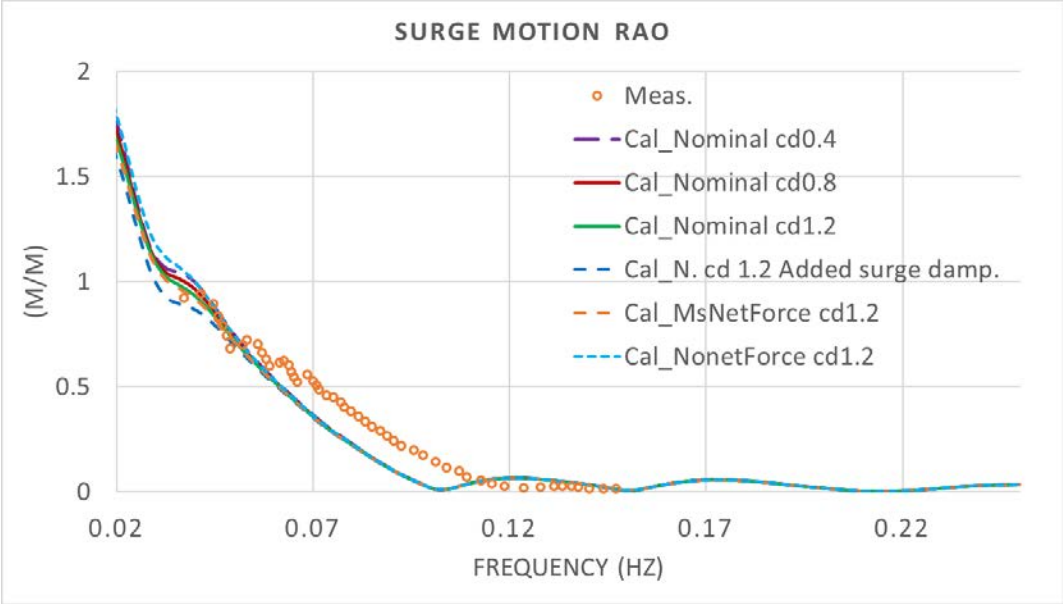

Fig. 13. Surge motion RAO, wave direction 180 deg.

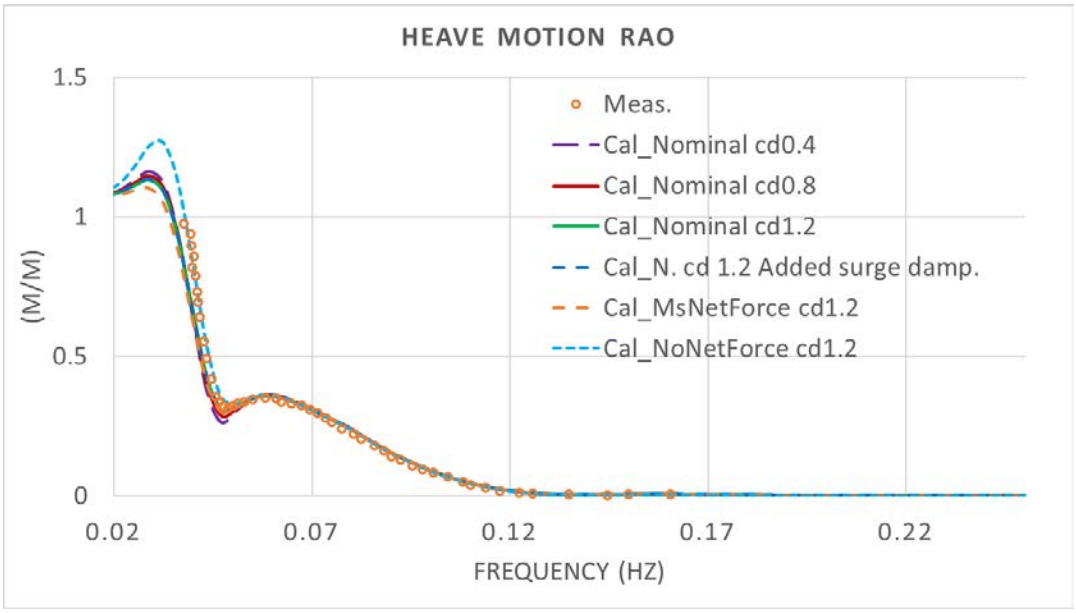

Fig. 14. Heave motion RAO, wave direction 180 deg.

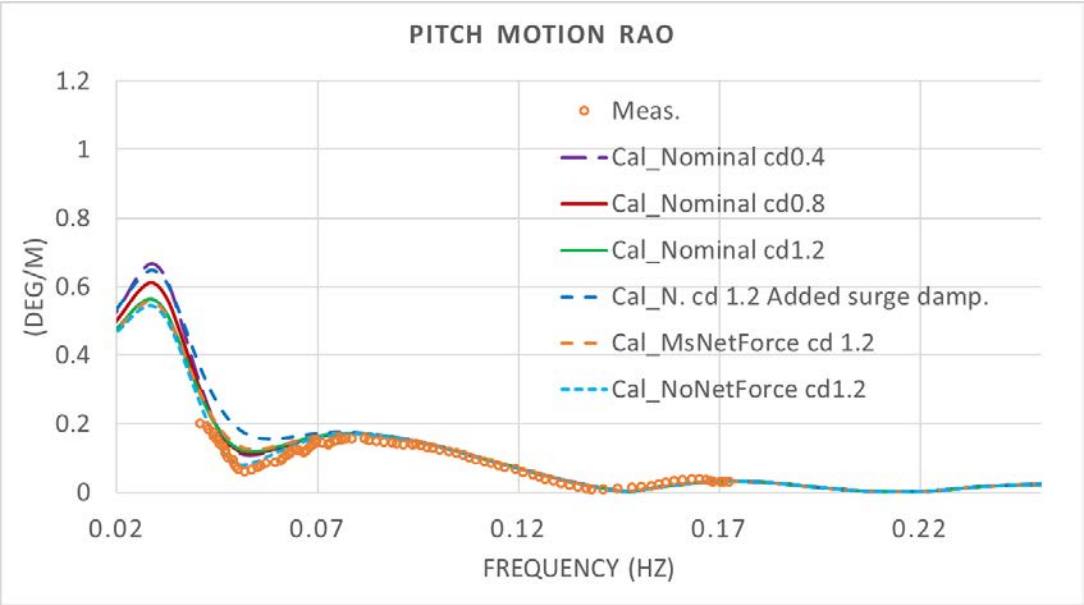

Fig. 15. Pitch motion RAO, wave direction 180 deg.

3.2. Results of numerical calculation and measurement in irregular waves and with/without current

The established numerical model is shown to give reasonable motion response estimation for the farm structure in the wave frequency range. In the following, the motion response of the farm structure in irregular waves and with/without current will be analyzed and discussed, where wind velocity is always zero.

The two-parameter JONSWAP wave spectrum is applied in model tests and numerical simulations. Measured and numerical (generated in SIMO/SIMA) wave spectra for Hs=5 m and Tp=11 s are shown in Fig. 16. The measured and numerical waves are close to each other except that the measured wave contains some more energy than the numerical wave around the wave peak period. A few test runs were performed in the time domain with both the measured wave time series and the numerical wave time series, the difference of the predicted farm motion is very small. Therefore, the numerical waves will be used in the following.

The model test results show there are significant motion response in the lower frequency range (lower than incoming wave frequency) for the surge and pitch motion. Heave motion is dominated by the wave frequency response though there is also motion response at its natural period. This section starts with a study on the excitation forces for the low frequency motion response. Then the farm motion in irregular waves without current is presented, followed by farm motion in both irregular waves and current conditions.

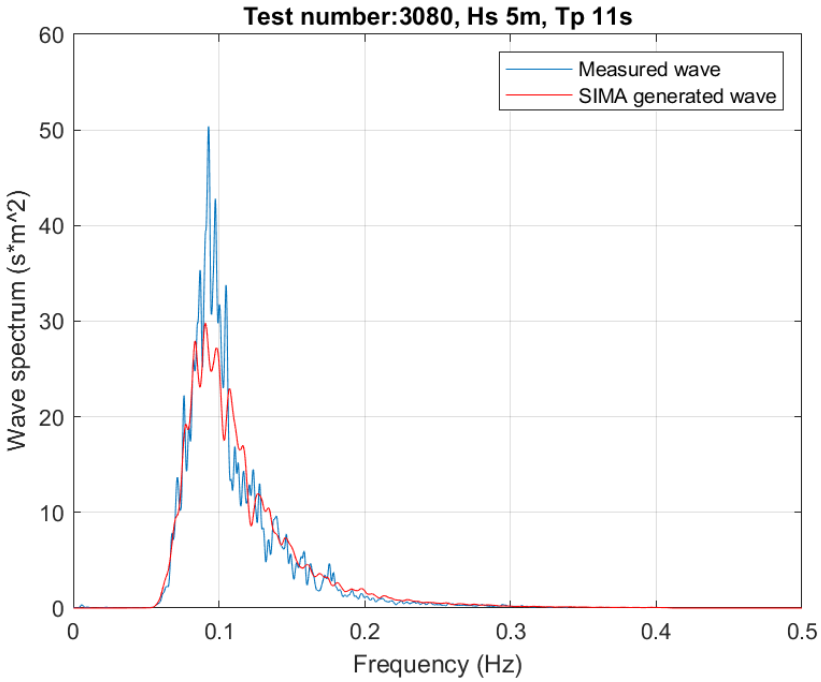

Fig. 16. Measured and numerical wave, two-parameter JONSWAP wave spectrum, Hs=5 m, Tp=11s.

3.2.1. Second order wave forces

For the low frequency surge and pitch motion, both second order wave force and viscous drag force can contribute to the excitations. With low damping in these frequency ranges, large motion occurs. To investigate the excitation and damping mechanism of the observed low frequency motion, the following work has been performed.

1) 6DOF mean drift forces are calculated using both WAMIT and HYDROSTAR [50]. Both WAMIT and HYDROSTAR provide three ways for mean drift calculation. The first one is the far field momentum flux method. With the far-field momentum flux method, it is only the 3 horizontal mean drift forces/moments can be evaluated. The second one is the control surface momentum flux method. WAMIT requires a complete control surface including the free surface if 6DOF mean drift forces are to be calculated. HYDROSTAR requires the control surface to be open at the free surface and it calculates only the horizontal mean drift forces and moment, with the control surface method (known as middle field method as well). The third one is direct body pressure integration method and with this method 6DOF mean drift forces can be calculated.

   In this study, the vertical motion modes are of interest (pitch motion) and the direct body pressure integration method is applied in mean drift force calculation. To quantify the calculation performed with body pressure integration method, far field momentum flux method is also applied for the mean horizontal drift force calculation. The comparisons of the calculated mean drift forces by the two different methods are shown in Figs. 17-19. Uni-direction wave is considered, and the wave direction is 180 degree.

   For the surge mean drift force, the two sets of HYDROSTAR calculation show very good agreement; the two sets of WAMIT calculation show deviation when the frequency is higher than 0.25 Hz; the WAMIT calculation using far-field method generally agrees well with the HYDROSTAR calculation.

The surge mean drift force calculated by direct pressure integration method with WAMIT is different from the rest calculations. This implies further convergence study is needed if the results of direct pressure integration method with WAMIT will be used. For the heave mean drift force, the WAMIT and HYDROSTAR calculations agree well, except the force calculated at heave natural frequency. For the pitch mean drift force, good agreement is observed between WAMIT and HYDROSTAR calculations.

With the calculated 6DOF mean drift forces imported to SIMO and with Newman's Approximation [51] applied to formulate the second order wave loads, both the first order and second order wave forces are taken into account in the time domain simulation. With Newman's approximation, the off-diagonal QTF terms are approximated by the diagonal terms and this saves computation time significantly. The motion responses of the Ocean Farm 1 structure with using the mean drift force – Newman's approximation method are analyzed and presented in the next section.

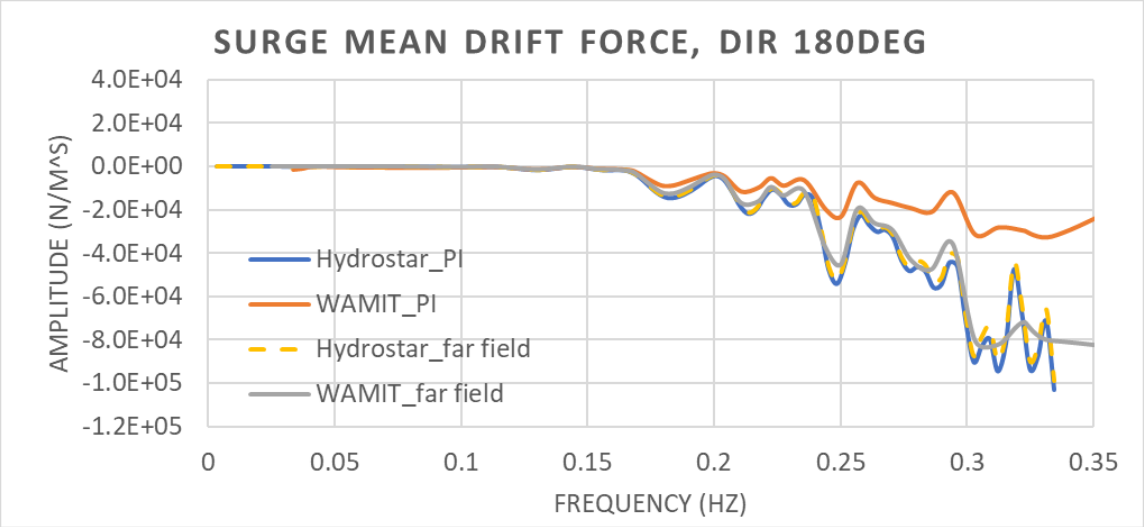

Fig. 17. Mean drift force in surge ("PI" denotes pressure integration method).

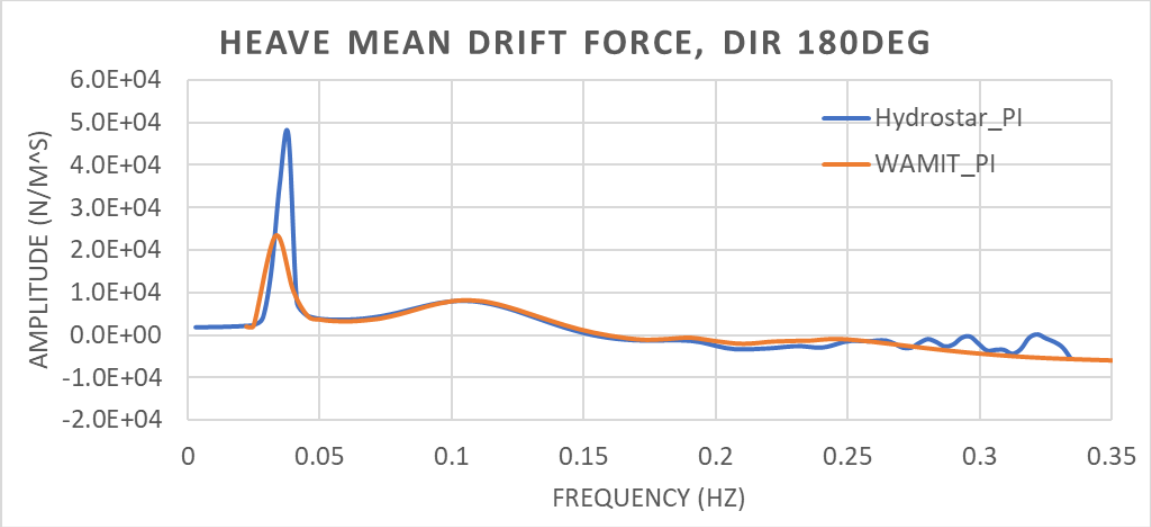

Fig. 18. Mean drift force in heave.

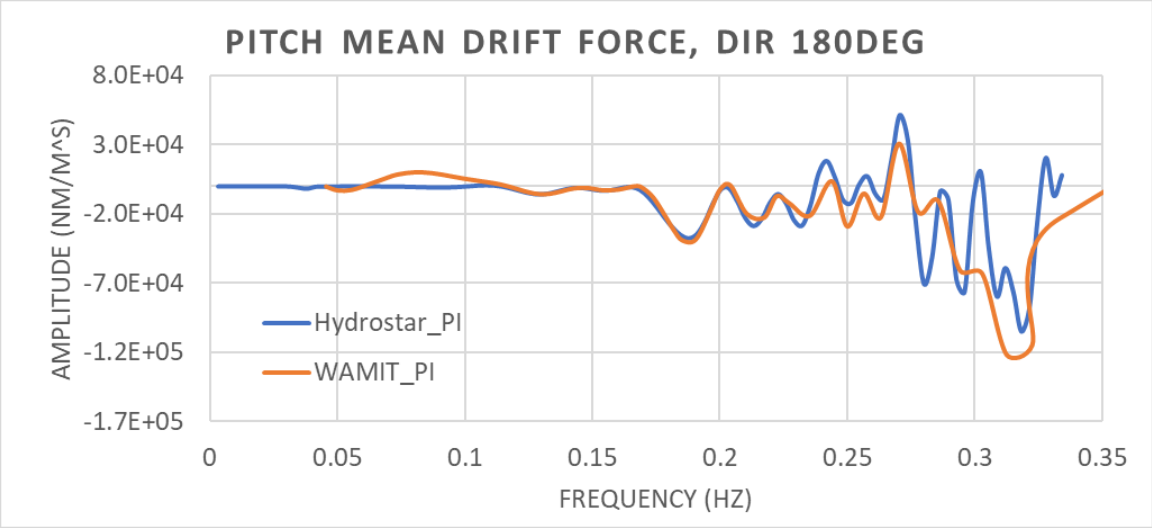

Fig. 19. Mean drift force in pitch.

2) Newman's approximation usually gives satisfactory results for slow-drift motions in the horizontal plane, since the natural period of the horizontal motion is normally much larger than the wave frequency. For slow-drift motions in the vertical plane, e.g. the heave/pitch motions of a floating structure, Newman's approximation may underestimate the slow-drift forces and in such case the solution of full QTF matrix is required. So, if slowly varying vertical motion is important or if the structure has relatively large natural frequencies, it is recommended to apply the full difference frequency QTFs [49]. Depending on the interested frequency range, one can further choose to perform difference-frequency QTF and sum-frequency QTF calculations. For the Ocean Farm 1 structure, the measurement shows that there are significant low frequency surge and pitch motion and the pitch motion natural period is around 30 s. So difference-frequency QTF calculation is performed in this study.

   Difference-frequency QTF is calculated using HYDROSTAR with the control surface method. For this method, HYDROSTAR requires that the control surface to be closed at the free surface (different from the mean drift calculation). The applied control surface is shown in Fig. 20. Diameter of the control surface on free surface is 150 m and the bottom control surface is 55 m below calm water surface. Quadrilateral mesh is used to discretize the control surface, number of meshes is listed in Table 13. The calculated surge, heave and pitch difference-frequency QTF at wave direction 180 deg are shown in Figs. 21-23.

   The surge difference-frequency QTF increases with the increase of incoming wave frequency; the force magnitude is largest along the diagonal and the force magnitude varies along the direction perpendicular to the diagonal. The heave QTF shows a similar trend as the surge QTF force. The magnitudes of the surge and heave QTF force are comparable. The magnitude of the pitch QTF increase with the incoming wave frequency as well. However, its magnitude is smallest along the diagonal. Along the direction perpendicular to the diagonal, the pitch QTF magnitude first increases and then decreases. For all the three degrees of freedom, the QTF magnitude is not smooth in the region close to the diagonal, especially for heave and pitch motions. This indicates that Newman's approximation may not be sufficient and QTF calculation is needed for the Ocean Farm 1 structure.

The calculated difference-frequency QTF is then imported into SIMO/SIMA to formulate the second-order wave load used in the time domain simulations. Motion response of the Ocean Farm 1 structure is studied with the calculated difference-frequency QTF and the results are shown in the following sections.

Table 13

Number of meshes used for the control surface for QTF calculation.

Surface component	Number of meshes
Free surface	32800
Bottom surface	22500
Side/vertical surface	7200
Complete control surface	62500

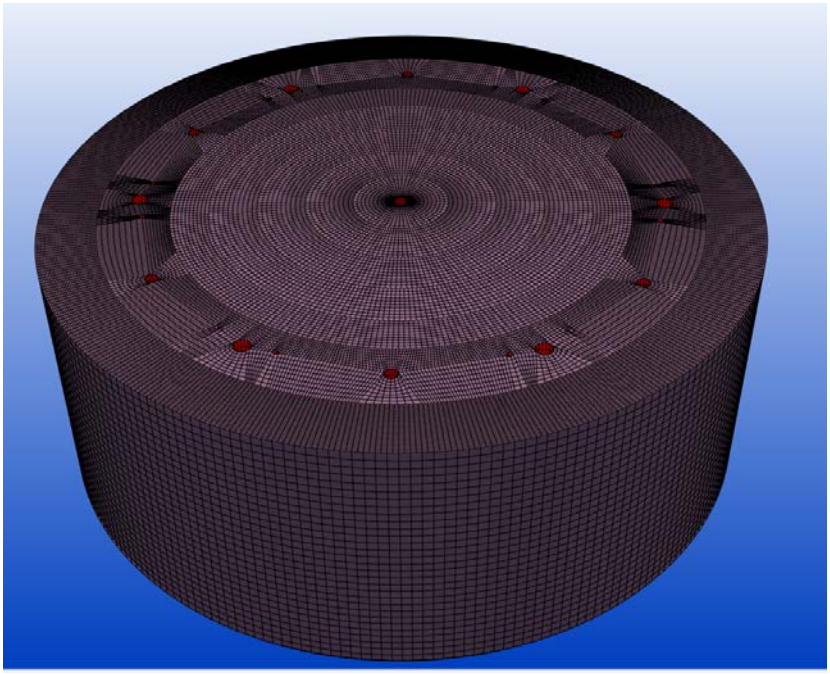

Fig. 20. Visualization of the control surface used for QTF calculation.

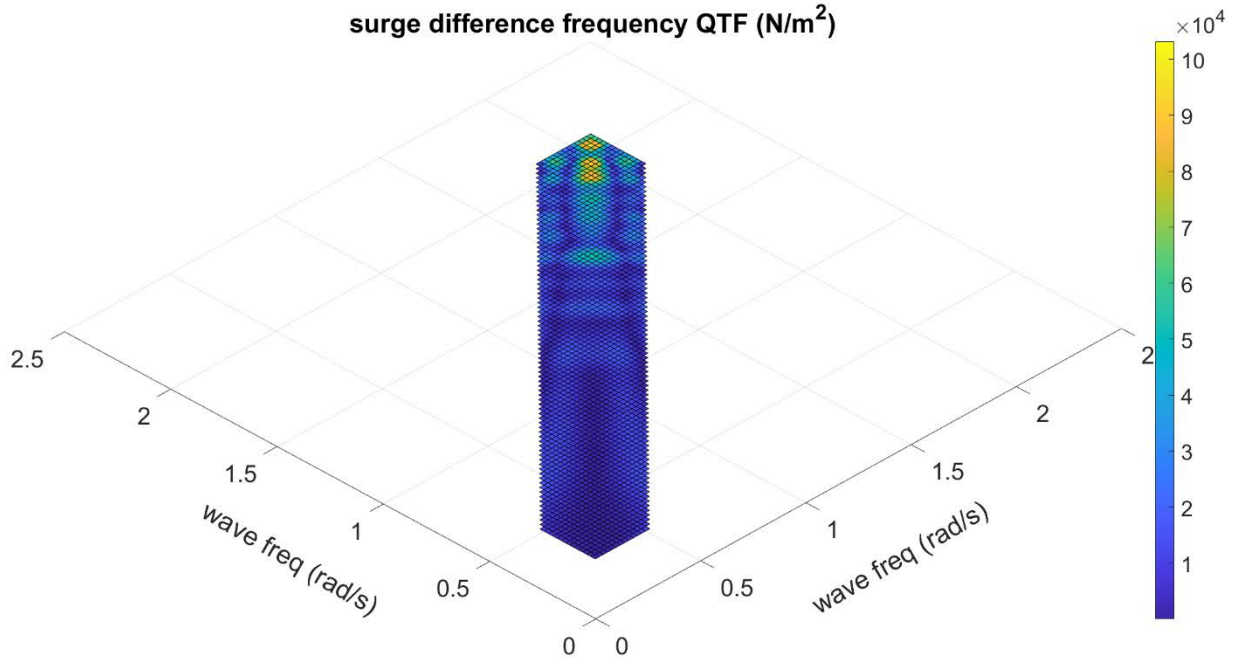

Fig. 21. Calculated surge QTF force in wave direction 180 deg.

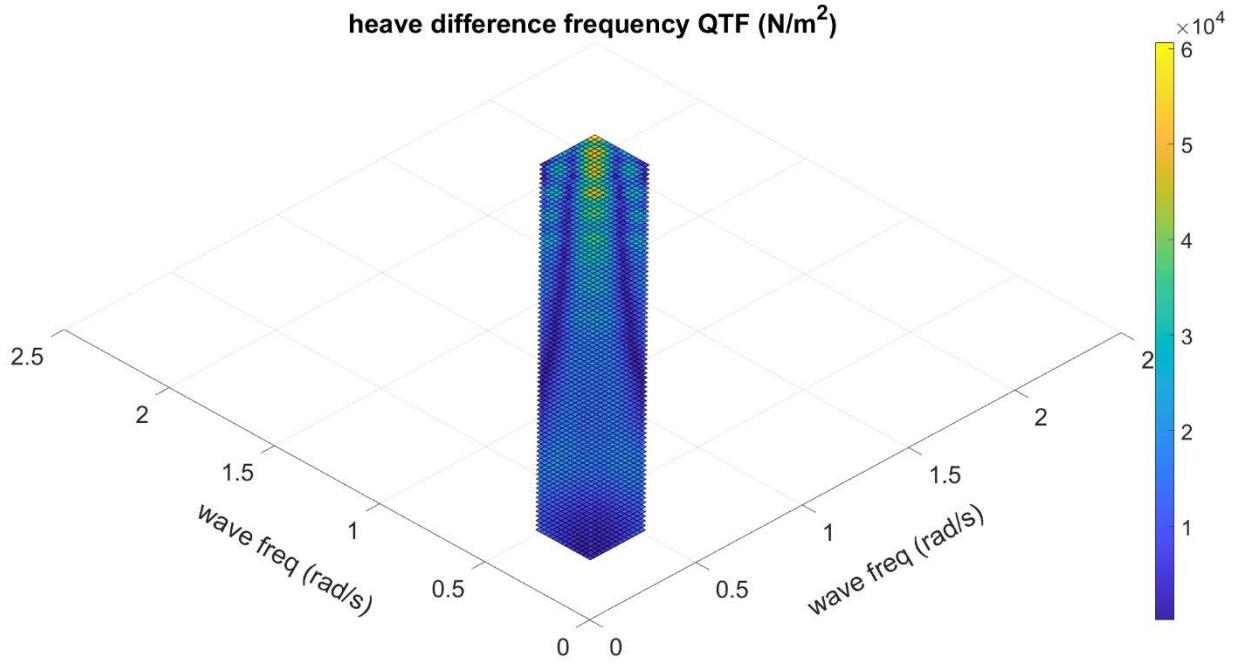

Fig. 22. Calculated heave QTF force in wave direction 180 deg.

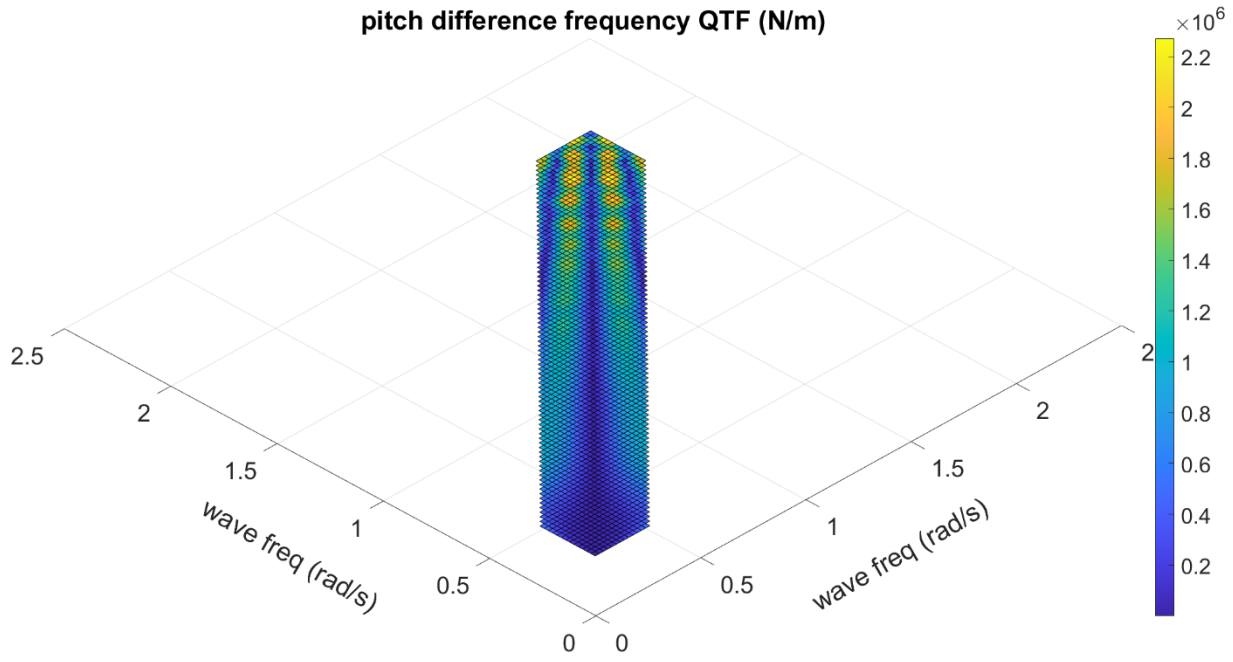

Fig. 23. Calculated pitch QTF force in wave direction 180 deg.

3) The Ocean Farm 1 structure consists of many slender structures so that the viscous drag load may play an important role in its motion responses. In addition to the second order wave forces, the viscous drag load may also excite the observed low frequency motions. As explained in the previous sections, viscous drag load is modeled for each column component of the farm structure. To illustrate the influence of drag load onto the farm motion, three drag coefficient values are considered in the following sections: 0.4, 0.8 and 1.2. Viscous load on the net also influences the motion response, which is determined based on empirical formulas dependent on the net solidity ratio, relative flow velocity/angle and Reynolds number. To illustrate the effect of viscous load on the net structure, numerical simulations are performed with/without net structure and with both model scale and full scale Reynolds numbers for a few chosen cases.

3.2.2. Calculated and measured motion response in irregular wave

Motion response analysis of the Ocean Farm 1 structure is performed in irregular waves. Four sea states are considered with Hs = 5 m, 4 m, 3 m and 1.5 m and wave direction is 180 degrees. The measured and calculated surge, heave and pitch motion standard deviation and mean surge motion are listed in Table 14, with two numerical models applied:

1) "Cal_Nominal cd0.8", with net load at full scale Reynolds number and column drag 0.8

2) "Cal_N. cd1.2 Added surge damp.", with net load at full scale Reynolds number, column drag 1.2 and additional surge damping added.

Difference-frequency QTF is applied in the SIMO time domain simulation. The comparison shows the numerical model captures the farm's heave and pitch motion magnitude reasonably well. For the surge motion,

the current numerical model seems to underestimate the damping and overestimate the motion response. The mean surge position is underestimated in wave only conditions.

Table 14

Motion statistics in irregular wave calculated vs. measured.

Hs (m)/ Tp(s)	Cur. vel. (m/s)	Dir. (deg)	Surge std. (m) cal.1)/ cal.2)/ meas.			Surge mean (m) cal.1)/ cal.2)/ meas.			Heave std. (m) cal.1)/ cal.2)/ meas.			Pitch std. (deg) cal.1)/ cal.2)/ meas.		
5/11	0	180	2.7	1.9	1.64	-0.34	-0.5	-3.3	0.20	0.19	0.21	0.25	0.23	0.29
4/10	0	180	2.0	1.4	0.96	-0.27	-0.3	-2.2	0.12	0.12	0.12	0.18	0.16	0.19
3/9	0	180	1.5	0.9	0.59	-0.2	-0.2	-1.4	0.06	0.06	0.06	0.12	0.1	0.11
1.5/7	0	180	0.6	0.4	0.19	-0.1	-0.1	-0.6	0.01	0.01	0.01	0.05	0.03	0.03

For the test case with Hs=5 m, numerical simulations using different formulations of the second-order wave forces are compared in Figs. 24-26, including the Newman's approximation method for mean drift force using both WAMIT and HYDROSTAR and with direct pressure integration method. Nominal numerical model with viscous load on frame structure and net structure is applied where column drag coefficient cd is 0.8 and net load is formulated based on full scale Reynolds number. For the surge motion, the motion responses at the very low frequency range are close to each other, except that a larger response is calculated by the QTF method at around 0.033Hz. When compared with measurement, the calculated surge motion responses by all of the three methods are larger than the measurement in the frequency range between 0.01Hz and 0.1Hz. For the heave motion, the mean drift force method underestimates the motion response at its natural frequency (around 0.037Hz) while the QTF method gives better estimation of the response at natural frequency. The measurement indicates there is some heave motion response at very low frequency range (below 0.01Hz), which is not observed from numerical simulations. For the pitch motion, the mean drift force method gives very small motion response at the pitch natural frequency (around 0.032Hz). The QTF method gives significantly larger motion response at the pitch natural frequency, which compares well with the measured motion response at the same frequency range. There is also large pitch response at the natural frequency of surge motion (around 0.006Hz) where large surge motion is also observed. The measured pitch response has a relatively flat energy distribution between the pitch and surge natural frequencies while the numerical calculated pitch motion shows two dominant peak response around the pitch and surge natural frequencies respectively and very low response between these two frequencies.

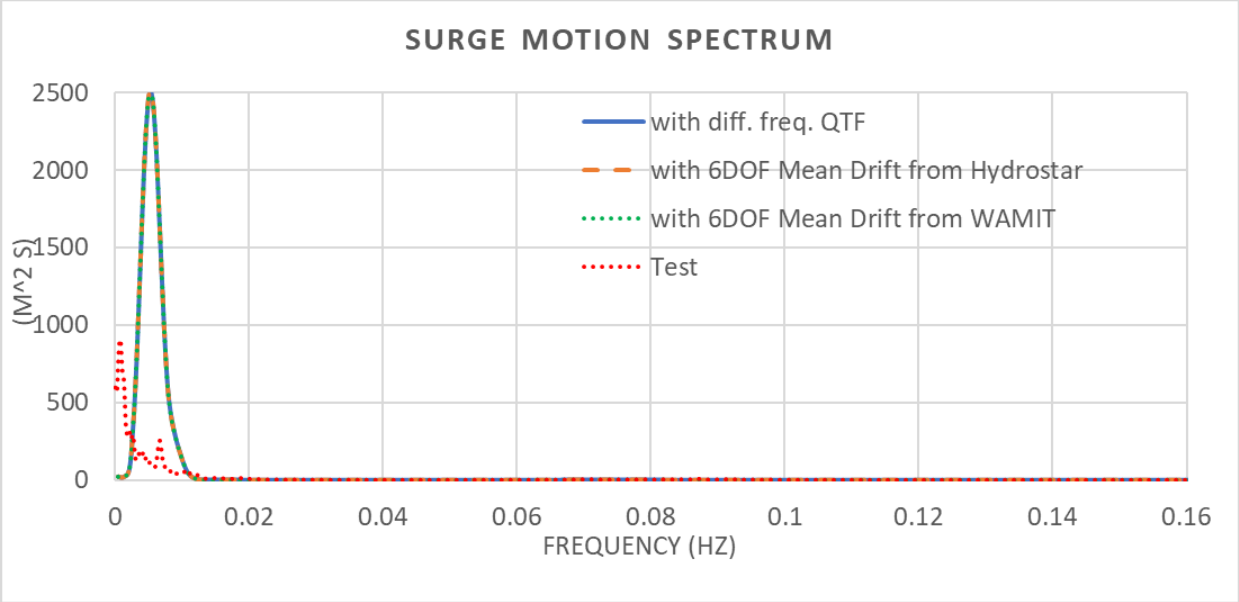

(a) Full spectrum

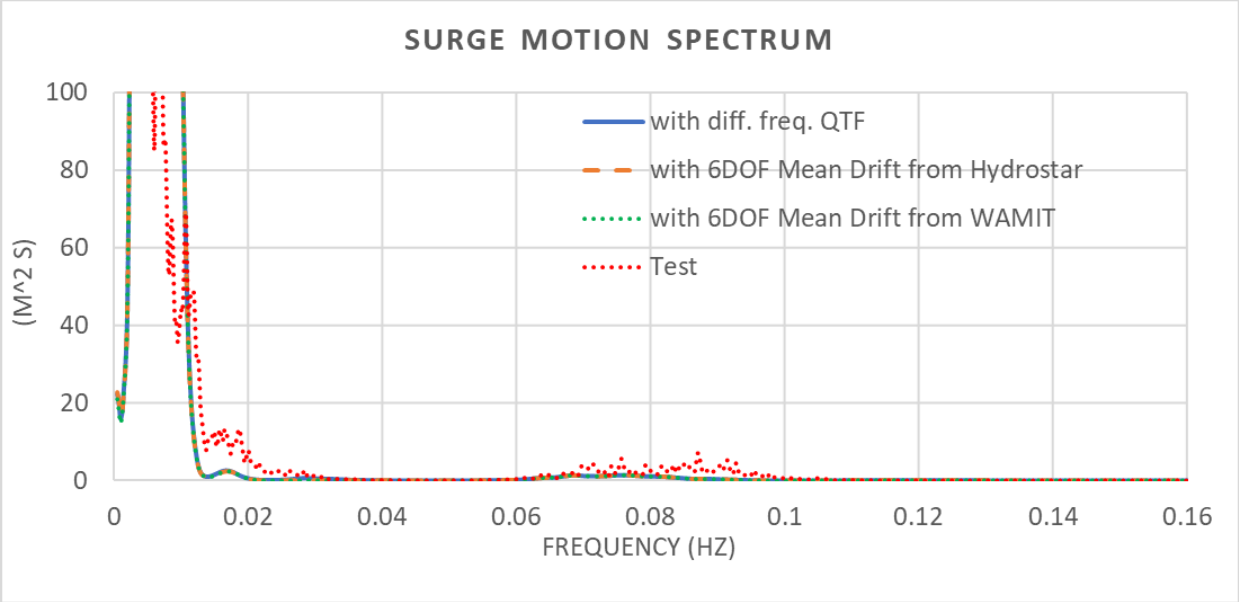

(b) Truncated spectrum with spectrum value up to 100 m^2/s

Fig. 24. Surge motion spectrum, Hs=5 m, current velocity=0 m/s, wave direction 180 deg.

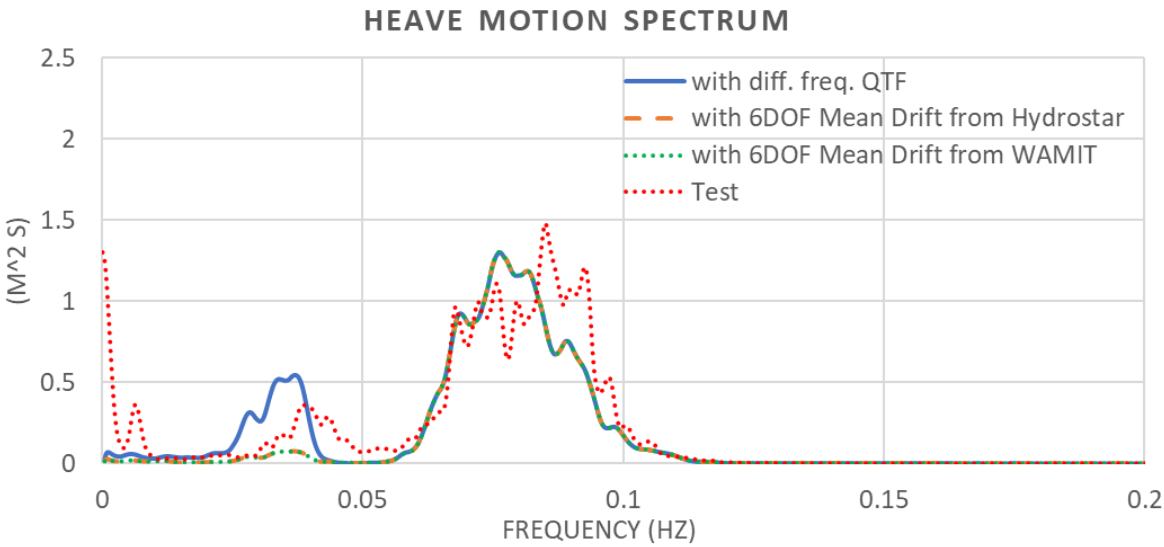

Fig. 25. Heave motion spectrum, Hs=5 m, current velocity=0 m/s, wave direction 180 deg.

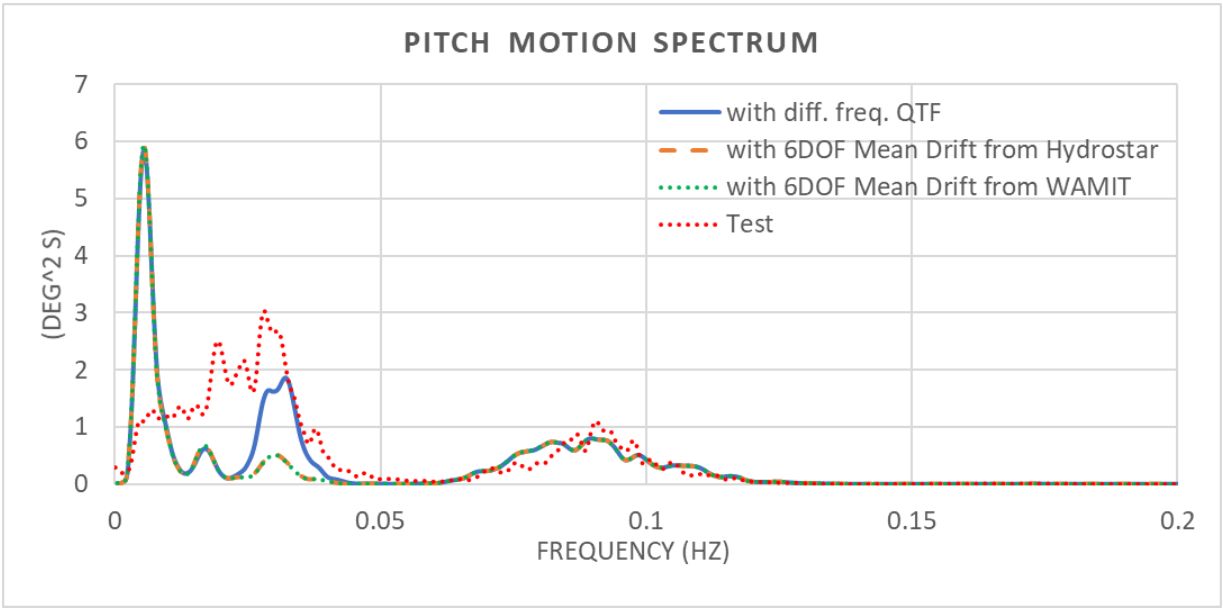

Fig. 26. Pitch motion spectrum, Hs=5 m, current velocity=0 m/s, wave direction 180 deg.

For the test case with Hs=5 m, numerical simulations are also performed with different drag coefficients applied on frame columns, with additional surge damping, without netload and with net load formulated using model scale Reynolds number, as shown in Figs. 27-29. The applied numerical models are summarized as below. The same set of numerical models are applied in section 3.2.3.

1) "Cal_Nominal cd0.4", with net load at full scale Reynolds number, column drag 0.4 and QTF
2) "Cal_Nominal cd0.8", with net load at full scale Reynolds number, column drag 0.8 and QTF
3) "Cal_NoNetForce cd0.8", without net load, with column drag 0.8 and QTF
4) "Cal_Nominal cd1.2", with net load at full scale Reynolds number, column drag 1.2 and QTF
5) "Cal_N. cd1.2 Added surge damp.", with net load at full scale Reynolds number, column drag 1.2, additional surge damping added and QTF

6) "Cal_MsNetForce cd1.2", with net load at model scale Reynolds number, column drag 1.2 and QTF

The base case for this set of comparison is with frame column drag coefficient cd=1.2, with QTF applied for second-order wave force formulation and with net load formulated using full scale Reynolds number. Each parametric study case is obtained by varying only one parameter of the base case while keeping the rest parameters the same, except the case ‘‘Cal_NoNetForce cd0.8’’ with two changes introduce to the based case. With the decrease of cd coefficient, the motion response at the natural frequencies increases significantly for the surge, heave and pitch motion. The net force also provides significant damping to the motion response at resonance frequency for the heave and pitch motion. The net force seems to be important for the excitation of low frequency surge motion. When the net is removed, the numerical calculation shows decreased surge motion response at its natural frequency. The added surge damping effectively reduces the surge motion at its natural frequency and corresponding pitch motion. Applying net load depending on model scale Reynolds number increases the surge motion response at its natural frequency and the corresponding pitch motion. Heave motion is not much influenced by either the added surge damping or the net load depending on model scale Reynolds number.

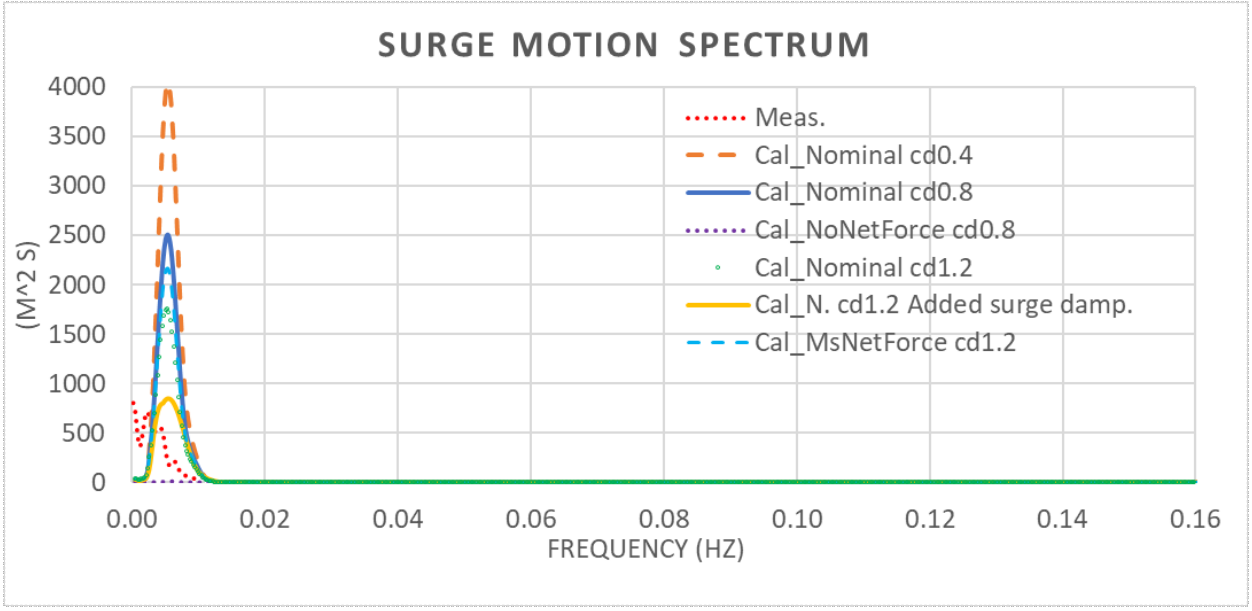

(a) Full spectrum

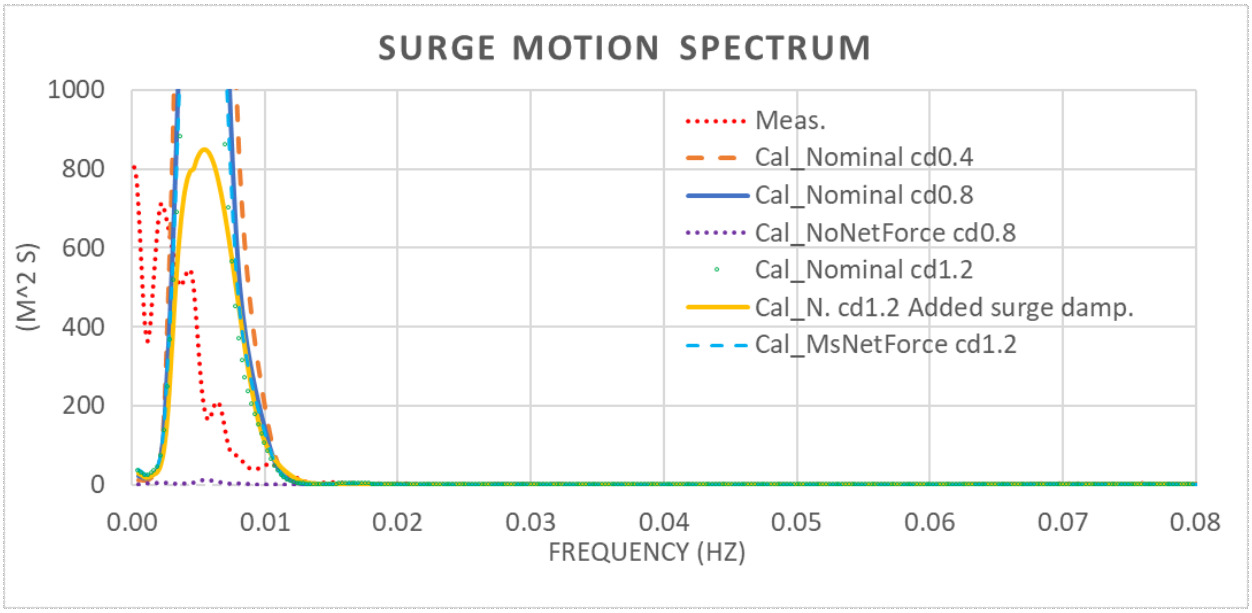

(b) Truncated spectrum with spectrum value up to 10 m^2/s

Fig. 27. Surge motion spectrum, Hs=5 m, current velocity=0 m/s, wave direction 180 deg, with different cd and with/without net structure.

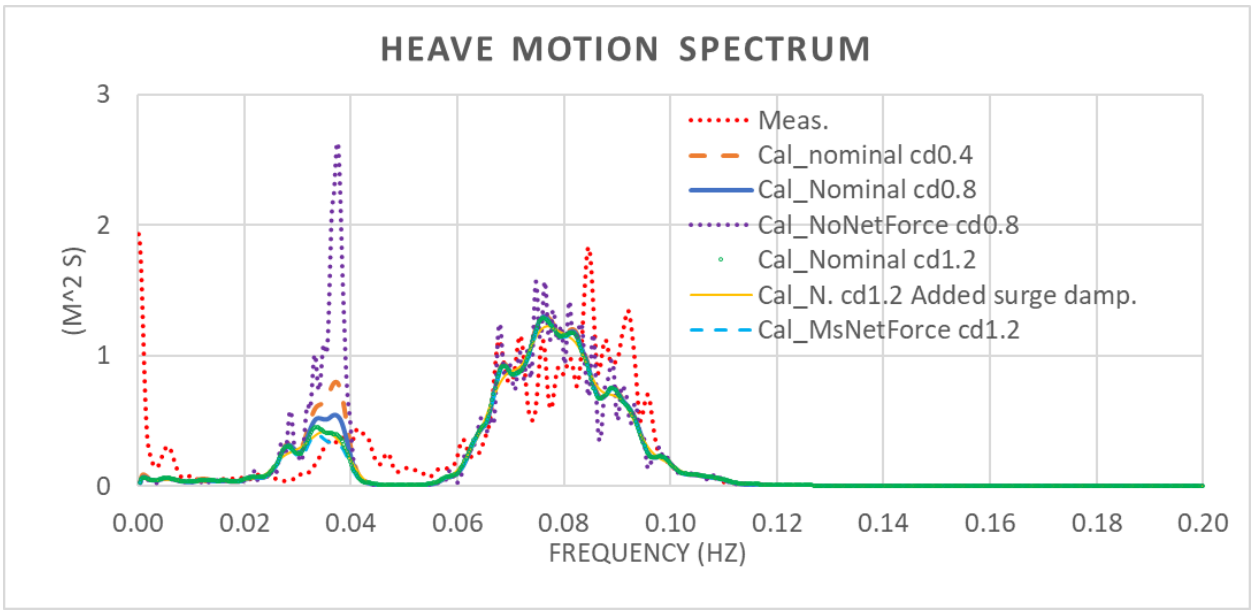

Fig. 28. Heave motion spectrum, Hs=5 m, current velocity=0 m/s, wave direction 180 deg, with different cd and with/without net structure.

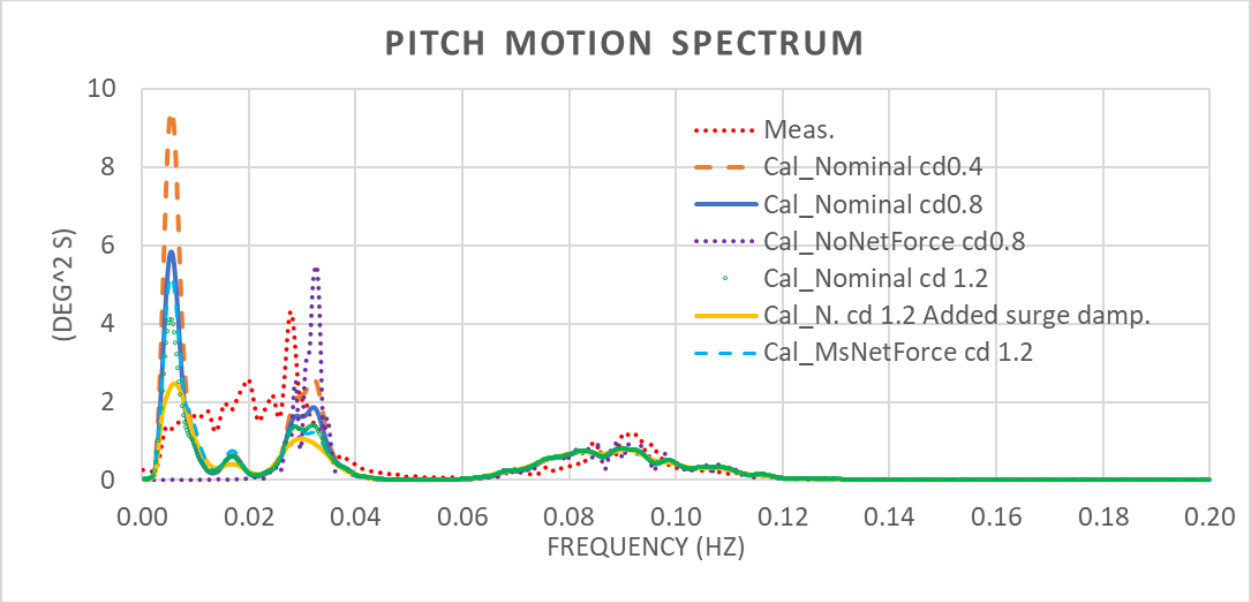

Fig. 29. Pitch motion spectrum, Hs=5 m, current velocity=0 m/s, wave direction 180 deg, with different cd and with/without net structure.

3.2.3. Calculated and measured motion response in combined irregular wave and current

Motion response of the Ocean Farm 1 model in combined irregular waves and current is studied and compared with measurement data. Motion standard deviation of surge, heave and pitch motion and mean surge motion is compared between numerical calculation and measurement for four sea states with Hs=1.5 m, 3 m, 4 m and 5 m, respectively. Wave and current are collinear, and the direction is 180 degrees. The same two numerical models as in the previous section are applied. The comparison results are presented in Table 15. Heave and pitch motion are reasonably estimated. Slight overestimation of surge motion standard deviation and mean position at higher sea states and underestimation of these response at lower sea states are observed.

For the sea state with Hs=5 m, the spectrum of measured and calculated surge, heave and pitch motions are compared and illustrated in Figs. 30-32. The cases of numerical calculations are the same as those used in the previous section. The comparisons show that wave frequency motion responses are well estimated by the numerical model and the motion response at individual natural frequencies are also captured by the numerical model. Calculated surge motion is dominated by the response at its natural frequency and the measured surge motion shows an over damped response without dominating peaks at its natural frequency. The calculated pitch motion shows response at the pitch and surge natural frequencies and at wave frequencies. The calculated response at pitch natural period seems to be over damped, and the calculated response at surge natural period seems not sufficiently damped. The heave motion is in general well predicted. The motion discrepancies at the surge natural frequency is related to surge damping estimation, which is a difficult task for Ocean Farm 1 type of structure consisting of many columns and net structure. A practical way forward might be to fine tuning the surge damping (linear and quadratic) in the numerical model to obtain good agreement of measured and calculated surge motion for a given sea state. The observed influence of frame column drag coefficients and net force (with/without net, model scale/full scale Reynolds number dependent net force) onto the farm motion are like those observed in the wave only cases. However, the added surge damping does not reduce the surge motion response at its natural frequency as much as those cases in wave only conditions (dot green line vs. solid orange line).

Table 15

Motion statistics in combined irregular wave and current, calculated vs. measured.

Hs (m)/ Tp(s)	Cur. vel. (m/s)	Dir. (deg)	Surge std. (m) cal.1)/ cal.2)/ meas.			Surge mean (m) cal.1)/ cal.2)/ meas.			Heave std. (m) cal.1)/ cal.2)/ meas.			Pitch std. (deg) cal.1)/ cal.2)/ meas.		
5/11	0.75	180	1.8	1.9	1.60	-26.5	-28	-23.6	0.19	0.19	0.21	0.32	0.29	0.35
4/10	0.75	180	1.6	1.5	1.22	-25.7	-27	-23.4	0.12	0.12	0.13	0.24	0.21	0.22
3/9	0.5	180	1.3	1.2	0.90	-15.48	-18	-16.6	0.06	0.06	0.06	0.15	0.14	0.15
1.5/7	0.25	180	0.64	0.6	1.08	-5.0	-6	-8.5	0.01	0.01	0.02	0.05	0.04	0.06

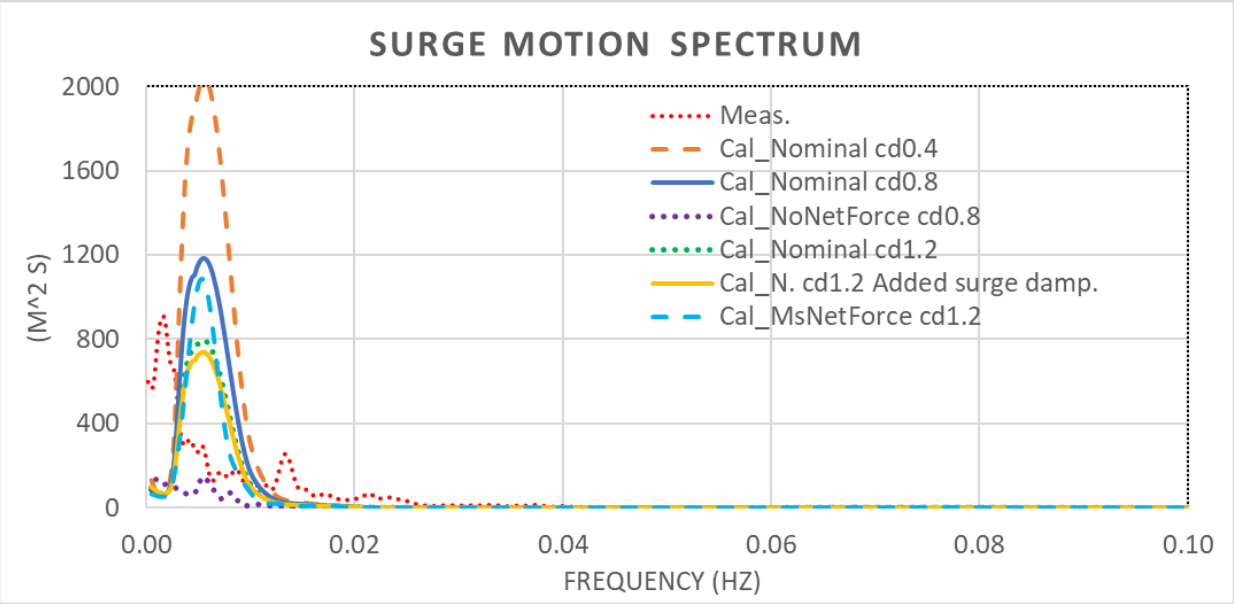

Fig. 30. Surge motion spectrum, Hs=5 m, current velocity=0.75 m/s, wave direction 180 deg, with/without net structure.

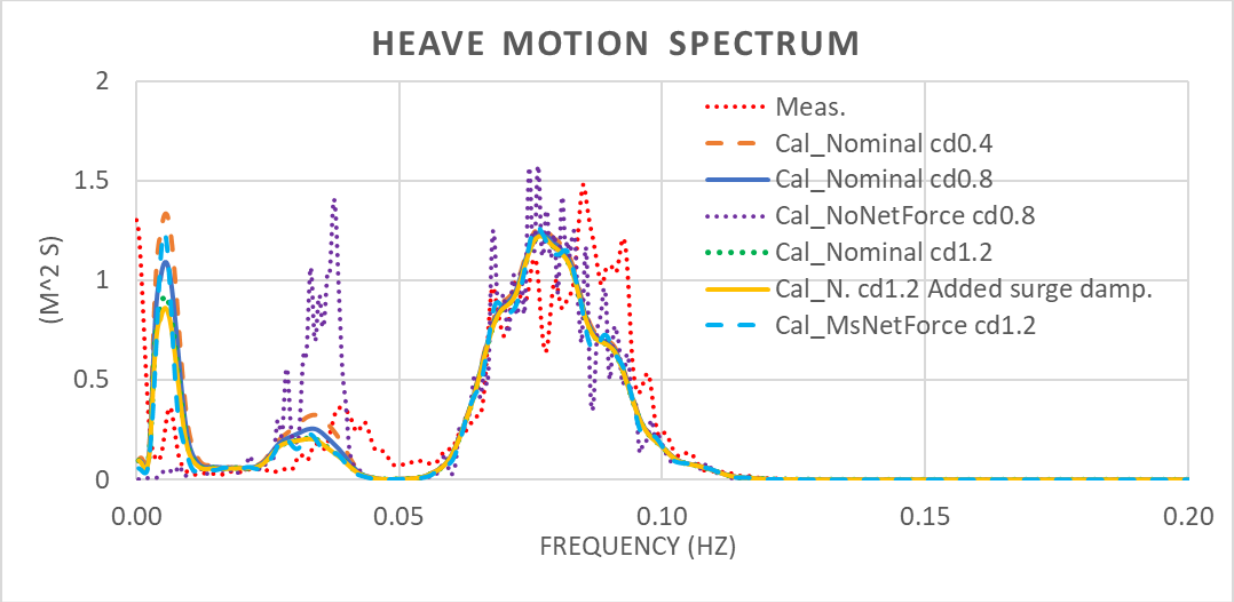

Fig. 31. Heave motion spectrum, Hs=5 m, current velocity=0.75 m/s, wave direction 180 deg, with/without net structure.

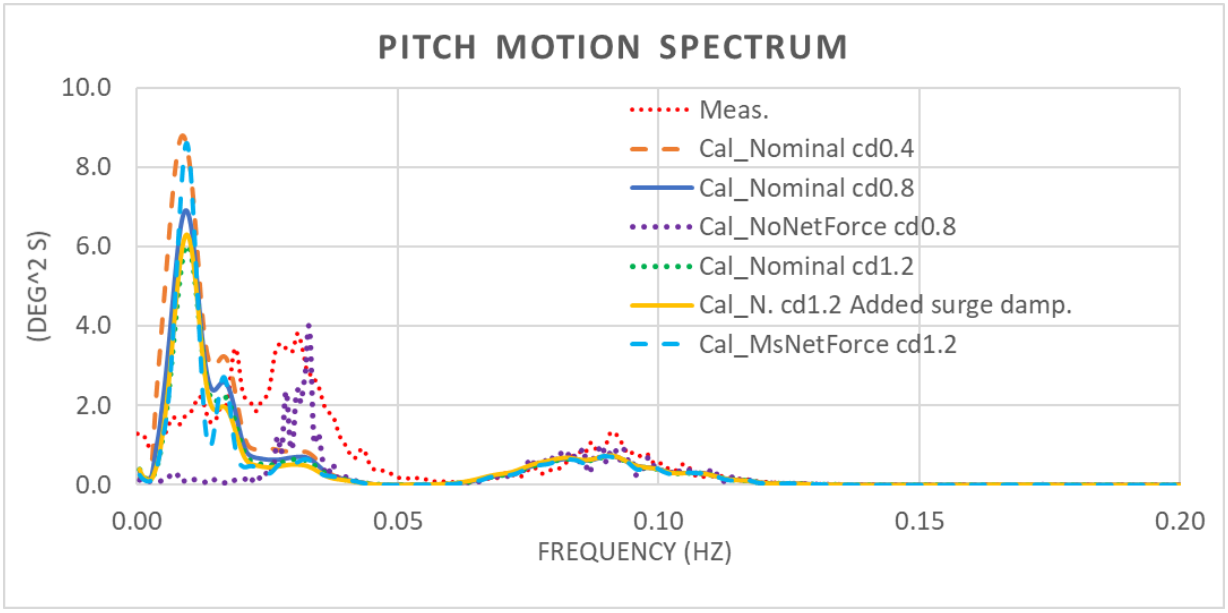

Fig. 32. Pitch motion spectrum, Hs=5 m, current velocity=0.75 m/s, wave direction 180 deg, with/without net structure.

4. Conclusions

A numerical modelling scheme has been proposed to model the loads and motion responses of Ocean Farm 1 in waves and current. The corresponding numerical model was established by using WAMIT, HYDROSTAR, SIMO and RIFLEX in SIMA. The time domain simulations are performed for motion prediction in waves and current. The added mass and damping force coefficients and the wave excitation forces for the frame structure of Ocean Farm 1 (no net) are calculated by using WAMIT. The quadratic drag load on the individual column of the frame structure influences the motion response and is modelled by using slender element in SIMO. The

viscous load on to the net is formulated by using the screen type force model. The calculation of the net force and the connection with SIMO time domain simulation is realized by using the Dynamic Linked Library in SIMO. The 8 mooring lines of Ocean Farm 1 are numerically modelled by using RIFLEX. The hydrodynamic load is formulated by using Morison's equation and the structural models are formulated by using FEM. A coupled RIFLEX-SIMO model is then established for the Ocean Farm 1 – mooring lines system.

The numerically predicted motion performance of Ocean Farm 1 is systematically compared with measurement data. The force - displacement of the mooring system and the natural periods of the surge/heave/pitch motion are numerically well predicted. The numerical model slightly underestimates the total damping for the resonant motion, especially for the surge decay motion. Offset in current is calculated at three current velocities 0.25/0.5/0.75 m/s and reasonable agreement against measured offset is obtained. The motion transfer functions are derived based on the motion response in pink noise wave spectrum, both in the numerical calculation and the measurement. The calculated motion transfer functions are in a reasonable agreement with the measurement, where the surge motion RAO is slightly underestimated, and the pitch motion RAO is overestimated in the frequency range [0.05-0.1 Hz].

The motion responses of the Ocean Farm 1 structure in irregular waves with/without current are further calculated and compared with measurement. Since the measurement shows significant surge and pitch motion response in the low frequency range outside wave frequency, the second-order wave forces are included in the numerical simulation. Further, two different ways are applied to formulate the second order wave forces: 6DOF mean wave drift force and Newman's approximation and difference-frequency QTF methods. To understand the influence of the different force components on the motion response, sensitivity studies are performed for different drag coefficients on the frame cylinders and with/without net load included.

The QTF method is able to predict the pitch motion response at its natural frequency while the mean drift – Newman's approximation method shows only very small pitch motion response at its natural frequency. The two methods give small difference in the predicted surge motion response. This implies that the Newman's approximation method is sufficiently good for estimating the surge/horizontal motion and the difference-frequency QTF method is needed to properly estimate the pitch motion response at its natural frequency. The drag coefficient of the frame column influences the motion responses at their natural frequencies. Net load also influences the motion response at the natural frequencies and in addition the net load is also an important excitation force for the low frequency pitch motion.

Standard deviation of heave and pitch motion is well predicted. Standard deviation of the surge motion is well predicted for the cases with current present and it is overestimated for the cases with zero current. The spectra analysis of the motion response indicates that the motion characteristics of the surge and heave motion are well captured. Surge motion is dominated by the response at its natural frequency. Heave motion is dominated by the response at wave frequencies and responses are also observed at its natural frequency. For the pitch motion, both measurement and numerical simulation indicates that the response at low frequency range is the dominant part. The numerical simulation gives two distinct response peaks around the surge and pitch natural frequencies respectively while the measurement indicates a rather evenly distributed energy between the surge and pitch natural frequencies.

The proposed numerical modelling scheme is verified through systematic comparison against model test measurement and the observed reasonable agreement. The obtained numerical results capture the main motion characteristics of the Ocean Farm 1 structure in calm water, current, regular waves, and irregular waves with/without current, in terms of motion standard deviation and dominating response frequencies. With this, the proposed scheme illustrates a practical way to tackle the hydrodynamic response of the Ocean Farm 1 structure, using commercially available software. The scheme can as well be generalized for other offshore fish farm structures consisting of a rigid frame structure and fish nets attached to it.

To further improve the proposed numerical modelling scheme, the following aspects might be considered. 1) To formulate the wave kinetics for net load calculation at instantaneous farm structure position. The wave

kinetics is formulated at the initial/equilibrium farm structure position in the current numerical model though the instantaneous farm structure velocity is taken into account when formulating the relative velocity. 2) To consider the instantaneous wave elevation in net load formulation. For the net panels close to the calm water surface, only the actual submerged part of the net panel shall contribute to the net load calculation. The close to surface net panel is assumed to be always submerged in the current numerical model. 3) To study of effect of wave drift damping onto the farm motion. As the surge motion is dominated by low frequency motion and the wave drift damping may be important in terms reflecting the change of the mean drift force for body with forward speed. 4) To perform more refined sensitivity study including sea-state and slender component dependent drag coefficient and current reduction effect on the net and frame structure in order to obtain more accurate motion estimation. In the current study, the same drag coefficient is applied for all the frame cylinders and all involved sea states. Current reduction effect is taken into account by introducing an empirical velocity reduction factor for the net structure at the leeward side.

Declaration of competing interest

The authors declare no conflicts of interest.

Acknowledgements

The authors are grateful to SALMA for the permission to publish this work. The authors would also like to acknowledge the Centre for Research-Based Innovation on Exposed Aquaculture Operations (SFI EXPOSED, funded by the Research Council of Norway, Project No. 237790), for financial support in writing the paper.

References

[1] Sjømat Norge Website, https://sjomatnorge.no/.

[2] Fredheim A, Langan R. Advances in technology for offshore and open ocean finfish aquaculture, New technologies in aquaculture: improving production efficiency and environmental management, Woodhead publishing series in food science, technology and nutrition; 2009. p. 914–944.

[3] Bjelland HV, Føre M, Lader P, Kristiansen D, Holmen IM, Fredheim A, Grøtli EI, Fathi DE, Oppedal F, Utne IB, Schjølberg I. Exposed aquaculture in Norway. In: Proceeding OCEANS 15 MTS/IEEE, Washington, USA; 2015.

[4] El-Thalji I. Context analysis of offshore fish farming. IOP Conference Series Materials Science and Engineering, 1st ProSES Symposium, 700: 012065, Kuantan, Pahang; 2019.

[5] Le Bris F, Marichal D. Numerical and experimental study of submerged supple nets applications to fish farms. Journal of Marine Science Technology 1998;3:161–170.

[6] Winther M. Optimization-based analysis of large cable-net structures for fishery. Doctoral Thesis, Aalborg University, Aalborg, Denmark; 2009.

[7] Moe H, Fredheim A, Hopperstad OS. Structural analysis of aquaculture net cages in current. Journal of Fluids and Structures 2010;26:503–516.

[8] Li L, Fu SX, Xu YW. Nonlinear hydroelastic analysis of an aquaculture fish cage in irregular waves. Marine Structures 2013;34:56–73.

[9] Kristiansen T, Faltinsen OM. Modelling of current loads on aquaculture net cages. Journal of Fluids and Structures 2012;34:218–235.

[10] Løland G. Current forces on flow through fish farms. Doctoral Thesis, The Norwegian Institute of Technology, Trondheim, Norway; 1991.

[11] Rudi H, Løland G, Furunes L. Model tests with net enclosures, forces on and flow through single nets and cage systems. Technical Report, MARINTEK, Trondheim, Norway; 1998.

[12] Lader P, Fredheim A. Dynamic properties of a flexible net sheet in waves and current – a numerical approach. Aquacultural Engineering 2006;35:228–238.

[13] Dou R. Numerical modelling and analysis of a semi-submersible fish cage. Master Thesis, Norwegian University of Science and Technology, Trondheim, Norway; 2018.

[14] Shen YG, Greco M, Faltinsen OM, Nygaard I. Numerical and experimental investigations on mooring loads of a marine fish farm in waves and current. Journal of Fluids and Structures 2018;79:115–136.

[15] Su B, Reite KJ, Føre M, Aarsæther KG, Alver MO, Endresen PC, Kristiansen D, Haugen J, Caharija W, Tsarau A. A multipurpose framework for modelling and simulation of marine aquaculture systems. In: Proceedings of the ASME 2019 38th International Conference on Ocean, Offshore and Arctic Engineering, Glasgow, Scotland; 2013.

[16] Marichal D. Cod-end numerical study. In: Proceedings of the 3rd International Conference on Hydroelasticity in Marine Technology, Oxford, UK; 2003.

[17] RIFLEX User Guide, version 4.16.0. SINTEF Ocean, Trondheim, Norway; 2019.

[18] Jin JZ, Selvik Ø, Yin DC, Yang X, Aksnes V, Fathi D. Review on typical marine operations in aquaculture and numerical simulation of one example operation scenario. In: Proceedings of the ISOPE 2018 28th International Ocean And Polar Engineering Conference, Sapporo, Japan; 2018.

[19] Kristiansen D, Faltinsen OM. Non-linear wave-induced motions of cylindrical-shaped floaters of fish farms. In: Proceedings of the Institution of Mechanical Engineers, Part M: Journal of Engineering for the Maritime Environment 2009;223:361–375.

[20] Li P, Faltinsen OM, Greco M. Wave-induced accelerations of a fish-farm elastic floater: experimental and numerical studies. In: Proceedings of the ASME 2014 33rd International Conference on Ocean, Offshore and Arctic Engineering, San Francisco, California, USA; 2014.

[21] Fu SX, Moan T. Dynamic analyses of floating fish cage collars in waves. Aquacultural Engineering 2012;47:7–15.

[22] Schubauer GB, Spangenberg WG, Klebanoff PS. National Advisory Committee for Aeronautics, Technical note 2001, Aerodynamic characteristics of damping screens. National Bureau of Standards, Washington, USA; 1950.
[23] Carrothers PJG, Baines WD. Forces on screens inclined to a fluid flow. Journal of Fluids Engineering 1975;97:116–117.
[24] Zhan JM, Jia XP, Li Y, Sun MG, Guo GX, Hu YZ. Analytical and experimental investigation of drag on nets of fish cages. Aquacultural Engineering 2006;35:91–101.
[25] Lader P, Jensen A, Sveen JK, Fredheim A, Enerhaug B, Fredriksson D. Experimental investigation of wave forces on net structures. Applied Ocean Research 2007;29:112–127.
[26] Zhao YP, Li YC, Dong GH, Gui FK, Wu H. An experimental and numerical study of hydrodynamic characteristics of submerged flexible plane nets in waves. Aquacultural Engineering 2008;38:16–25.
[27] Ito S, Kinoshita T, Kitazawa D, Bao W, Itakura H, Nishizawa S. Experimental investigation and numerical modelling of hydrodynamic force characteristics of a heaving net. In: Proceedings of the ASME 2010 29th International Conference on Ocean, Offshore and Arctic Engineering, Shanghai, China; 2010.
[28] Fu SX, Xu YW, Hu K, Zhong Q, Li R. Experimental investigation on hydrodynamics of a fish cage floater-net system in oscillatory and steady flows by forced oscillation tests. Journal of Ship Research 2014;58:20–29.
[29] Lader P, Enerhaug B. Experimental investigation of forces and geometry of a net cage in uniform flow. Journal of Oceanic Engineering 2005;30:79–84.
[30] Nygaard I. Merdforsøk, kapasitets-tester, interaksjon mellom not og utspilingssystem. Technical Report, MARINTEK, Trondheim, Norway; 2013.
[31] Kristiansen T, Faltinsen OM. Experimental and numerical study of an aquaculture net cage with floater in waves and current. Journal of fluid and structures 2015;54:1–26.
[32] Li L, Jiang ZY, Wang JG, Ong MC. Numerical study on the heading misalignment and current velocity reduction of a vessel-shaped offshore Fish Farm. Journal of Offshore Mechanics and Arctic Engineering 2019;141(5):051602.
[33] Nygaard I. Nordlaks Havfarm model tests. Technical Report, SINTEF OCEAN, Trondheim, Norway; 2018.
[34] Li L, Ong MK. A Preliminary Study of a Rigid Semi-Submersible Fish Farm for Open Seas. In: Proceedings of the ASME 2017 36th International Conference on Ocean, Offshore and Arctic Engineering, Trondheim, Norway; 2017.
[35] Bore PT, Fossan PA. Ultimate and fatigue limit state analysis of rigid offshore aquaculture structures. Master Thesis, Norwegian University of Science and Technology, Trondheim, Norway; 2015.
[36] USFOS User Manual. MARINTEK, Trondheim, Norway; 1999.
[37] SIMO User Guide, version 4.16.0. SINTEF OCEAN, Trondheim, Norway; 2019.
[38] SIMA, SINTEF Ocean's Integrated Simulation Environment, Version 3.7.0. SINTEF OCEAN, Trondheim, Norway; 2019.
[39] Sesam User Manual, HydroD, Wave load & stability analysis of fixed and floating structures, version 4.10. DNV GL, Oslo, Norway; 2017.
[40] Nygaard I. Ocean Fish Farm, model tests. Technical Report, MARINTEK, Trondheim, Norway; 2014.
[41] Zhao YP, Guan CX, Bi CW, Liu HF, Cui Y. Experimental investigations on hydrodynamic responses of a semi-submersible offshore fish farm in waves. Journal of Marine Science and Engineering 2019;7:238.
[42] WAMIT User Manual, Version 7.0. WAMIT, Inc., Chestnut Hill, MA, USA; 2013.
[43] Bore PT, Amdahl J, Kristiansen D. Modelling of hydrodynamic loads on aquaculture net cages by a modified Morison model. In: Proceedings of the 7th Internal Conference on Computational Methods in Marine Engineering, Nantes, France; 2017.
[44] Huang CC, Tang HJ, Liu JY. Dynamical analysis of net cage structures for marine aquaculture: Numerical simulation and model testing. Aquacultural Engineering 2006;35:258–270.

[45] Cheng H, Li L, Aarsæther KG, Ong MC. Typical hydrodynamic models for aquaculture nets: A comparative study under pure current conditions. Aquacultural Engineering 2020;90:102070.
[46] Shen YG. Operational limits for floating-collar fish farms in waves and current, without and with well-boat presence. Doctoral Thesis, Norwegian University of Science and Technology, Trondheim, Norway; 2018.
[47] Goldstein S. Modern developments in fluid dynamics – An account of theory and experimental relating to boundary layers, turbulent motion and wakes. Dover Publications, New York, USA; 1965.
[48] RIFLEX User Guide, version 4.16.0. SINTEF Ocean, Trondheim, Norway; 2019.
[49] Recommended Practice DNV-RP-C205: Environmental Conditions And Environmental Loads. DNV GL, Oslo, Norway; 2010.
[50] HYDROSTAR For Experts, User Manual, version 7.3, Bureau Veritas, Neuilly-Sur-Seine, France; 2019.
[51] Newman JN. Marine Hydrodynamics. Cambridge University Press; 1977.